SANDIA REPORT

SAND2007-4984
Unlimited Release
Printed September 2007

CHARICE 1.0: An IDL Application for Characteristics-Based Inverse Analysis of Isentropic Compression Experiments

Jean-Paul Davis

Prepared by
Sandia National Laboratories
Albuquerque, New Mexico 87185 and Livermore, California 94550

Sandia is a multiprogram laboratory operated by Sandia Corporation,
a Lockheed Martin Company, for the United States Department of Energy's
National Nuclear Security Administration under Contract DE-AC04-94AL85000.

Issued by Sandia National Laboratories, operated for the United States Department of Energy by Sandia Corporation.

Available to DOE and DOE contractors from
U.S. Department of Energy
Office of Scientific and Technical Information
P.O. Box 62
Oak Ridge, TN 37831

Telephone: (865)576-8401
Facsimile: (865)576-5728
E-Mail: reports@adonis.osti.gov
Online ordering: http://www.osti.gov/bridge

Available to the public from
U.S. Department of Commerce
National Technical Information Service
5285 Port Royal Rd
Springfield, VA 22161

Telephone: (800)553-6847
Facsimile: (703)605-6900
E-Mail: orders@ntis.fedworld.gov
Online order: http://www.ntis.gov/help/ordermethods.asp?loc=7-4-0#online

SAND2007-4984
Unlimited Release
Printed September 2007

CHARICE 1.0: An IDL Application for Characteristics-Based Inverse Analysis of Isentropic Compression Experiments

Jean-Paul Davis
Dynamic Material Properties
Sandia National Laboratories
P.O. Box 5800
Albuquerque, NM 87185-1181

Abstract

CHARICE is a multi-platform computer application that analyzes velocity waveform data from ramp-wave experiments to determine a material's quasi-isentropic loading response in stress and density using an iterative characteristics-based approach. The application was built using ITT Visual Information Solutions' Interactive Data Language (IDL®), and features graphical interfaces for all user interaction. This report describes the calculation method and available analysis options, and gives instructions for using the application.

This page intentionally left blank.

Contents

This page intentionally left blank.

Nomenclature

C_σ , C_u	phase velocities for disturbance in longitudinal stress and particle velocity
c_L	Lagrangian wave speed, equal to sound speed for simple wave
δc_L	uncertainty in Lagrangian wave speed from propagation of experimental uncertainties
c_0	sound speed at ambient condition
F	material state function $\int d\sigma_x / \rho_0 c_L$ used in Riemann invariants
FC_i, δFC_i	fringe count for measurement at sample *i*, and its experimental uncertainty
(*ineg*, *ipos*)	indices to intersection of negative characteristic *ineg* and positive characteristic *ipos*
ρ	density
ρ_0	density at ambient condition
σ_x	longitudinal stress
σ_R	longitudinal stress at the sample's right boundary
R^+, R^-	Riemann invariants along positive and negative characteristics
t	time
Δt	local spacing between time points
δt_i	experimental uncertainty in time for sample *i*
δT_i	total time uncertainty for sample *i* after folding in velocity uncertainty
t_{min}	left-hand boundary of time domain
u_g	in-situ velocity at the interface position defined on a uniformly-spaced velocity grid
u_p	particle (material) velocity
u^*	velocity along the principal compression isentrope due to a simple compression wave
$\delta u_i(u_p)$	experimental uncertainty in the measured interface velocity
v	specific volume
v_0	specific volume at ambient condition
VPF_i, δVPF_i	velocity-per-fringe of interferometer for sample *i*, and its experimental uncertainty

x_i, δx_i	initial thickness of sample *i*, experimental uncertainty in that thickness
δx_b	difference from nominal baseplate thickness
X	Lagrangian position
δX_i	total thickness uncertainty for sample *i* after folding in time and velocity uncertainties
X_L	Lagrangian position of sample's left boundary (side driven by ramp wave)
X_R	Lagrangian position of sample's right boundary (location of velocity measurement)
X_{Rmin}	Lagrangian position of the thinnest sample's right boundary

1. Introduction

CHARICE (**CHAR**acteristics-based analysis of **I**sentropic **C**ompression **E**xperiments) is a computer software application that implements an iterative Lagrangian analysis approach using backward characteristics solutions to analyze velocity-interferometry data from planar-geometry ramp-loading experiments and deduce a sample material's mechanical response under quasi-isentropic compression. This technique, described originally by Stephen Rothman and John Maw,[1–3] accounts for ramp-wave interactions arising from mismatched acoustic impedances at the measurement interface; velocity is typically measured at a free surface of the sample material, or at the interface between the sample material and a transparent interferometer window material. Given two or more velocity-time profiles representing particle velocity measurements on the back sides of different-thickness samples (all having been subjected to the same front-side loading history), CHARICE makes an initial guess at the in-situ velocity-time profiles that would occur at the measurement locations in semi-infinite samples, and an initial guess at the material response by performing Lagrangian analysis of these in-situ profiles. Then CHARICE iteratively computes improved estimates of the material response by using the previous result for material response to convert measured velocity profiles to improved estimates of the in-situ profiles, applying Lagrangian analysis to the new in-situ profiles. The conversion from measured to in-situ velocity profiles is accomplished by computing backward characteristics solutions through the wave-interaction region, then projecting characteristics forward from the undisturbed region for the case of a semi-infinite sample. Iteration continues until the relative change in the material response meets a stopping criterion.

The iterative approach taken by CHARICE differs significantly from the minimization approach developed by Dennis Hayes[4–7] and implemented by this author in the computer code INVICE.[8] While CHARICE represents material response with tabular data, determined by Lagrangian analysis of numerically-represented velocity profiles, the minimization technique requires an analytical model of the material response; values for the model's parameters are determined by minimizing the difference between backward-computed in-situ profiles at a point outside the interface's region of influence (not projected forward again to the measurement location). A tabular representation of material response can be advantageous in that the result is independent of any model, an important consideration when it is not clear what model would best represent the material under study. In many cases, the tabular representation makes it easy to capture the elastic-plastic transition region of the material response. The disadvantage of a tabular representation is that, from a practical standpoint, material response is restricted to a single-valued function (no dependence on history, time, strain-rate, *etc.*). A more obvious advantage of the iterative approach in CHARICE is speed; it typically achieves convergence with fewer than 10 backward calculations for each profile, compared to greater than 100 calculations for the minimization approach. The technique used to obtain backward solutions also differs between CHARICE, which uses characteristics, and INVICE, which uses a finite-difference scheme. The principal advantage of the characteristics-based technique is speed, but it cannot be applied to more than a single material layer as can the finite-difference technique.

An important feature of CHARICE is a graphical user interface (GUI) to control all aspects of the analysis. The application was written using ITT Visual Information Solutions' Interactive Data Language (IDL®), which allows it to run on multiple computing platforms using the freely available IDL Virtual Machine.™

Section 2 of this report describes in detail the methods used by CHARICE, while Sections 3 and 4 explain how to set up and run an analysis *via* the graphical user interface, including the sequence of operations CHARICE actually performs. Section 5 presents several examples to demonstrate the application. Sections 6 and 7 discuss limitations and suggest future extensions. The appendices provide information on the preference settings, setup file format, and installation details.

This page intentionally left blank.

2. Analysis Methods

The inverse analysis technique implemented in CHARICE has two main steps: Lagrangian analysis of in-situ velocity-time profiles, and mapping of measured velocity profiles to in-situ velocity profiles by use of a backward characteristics solution. An iterative approach is required because each step depends on results from the other step. The two steps are described separately in Sections 2.1 and 2.2. Methods for propagating experimental uncertainties to the final result for material response are discussed in Section 2.3. The analysis technique requires that all samples are subjected to identical front-side loading histories. Section 2.4 presents a method to approximately correct for one source of non-identical loading histories frequently encountered in magnetically driven isentropic compression experiments: unequal thicknesses of the baseplates on which samples are mounted.

2.1. Iterative Lagrangian Analysis

Lagrangian analysis is a technique previously developed [9 – 13] to determine material response from multiple in-situ gauges (measuring either longitudinal stress or particle velocity) positioned inside a single material sample, typically for impact experiments where the properties of the sample material cause a shock wave to evolve into a structured wave. The analysis is straightforward when the wave propagates as either a simple wave or steady wave, because the phase velocities $C_\sigma = (\partial X/\partial t)_\sigma$ for longitudinal stress and $C_u = (\partial X/\partial t)_u$ for particle velocity (X is Lagrangian coordinate) are then identical. For isentropic flow, these are equal to the Lagrangian wave speed c_L. For a simple wave, contours of σ_x and u_p in the X-t plane are straight lines, and σ_x is a function of only u_p. Measurement of in-situ velocity histories at two or more values of X gives c_L as a function of u_p by inverting the profiles to get $t(u_p)$ and fitting, for each value of u_p, a straight line through a set of points in the X-t plane. Material response in terms of specific volume and longitudinal stress is then determined by integrating

$$dv = -du_p/\rho_0 c_L(u_p) \qquad \text{and} \qquad d\sigma_x = \rho_0 c_L(u_p)du_p \tag{1}$$

along the velocity history at a fixed X (*i.e.*, a particular gauge location). Any dependence on rate, history, or entropy, however, produces non-simple flow with curved contours. Analysis of non-simple waves is possible by fitting piece-wise continuous surfaces to multiple-gauge data, but uniqueness becomes an issue.

In-situ measurements are very difficult to realize for typical ramp-loading experiments due to issues of sample size and opacity as well as electromagnetic or radiation environments. Instead, interferometric techniques are used to simultaneously measure particle velocity histories at the rear surfaces of multiple samples subjected to the same loading. These rear surfaces necessarily constitute interfaces with either vacuum (a free surface) or a transparent window material (unless the sample material is itself transparent and can be used as a window). The discontinuity in acoustic impedance at such an interface causes wave reflections that interact with the remainder of the oncoming ramp wave to create a region of non-simple flow near the interface, as illustrated schematically in Figure 1. These interaction regions preclude Lagrangian analysis as described in the previous paragraph.

The lines in Figure 1 represent characteristics, whose local slope is equal to the speed of propagation for disturbances. In regions of simple flow, the characteristics are straight and equal to contours of constant particle velocity. The interaction between reflected and incident characteristics bends the incident characteristics according to the local state of the material. Thus, the in-situ velocity that would occur at the interface position in a semi-infinite sample differs from the interface velocity not only in magnitude (due to the impedance mismatch), but also in arrival time for each value of veloc-

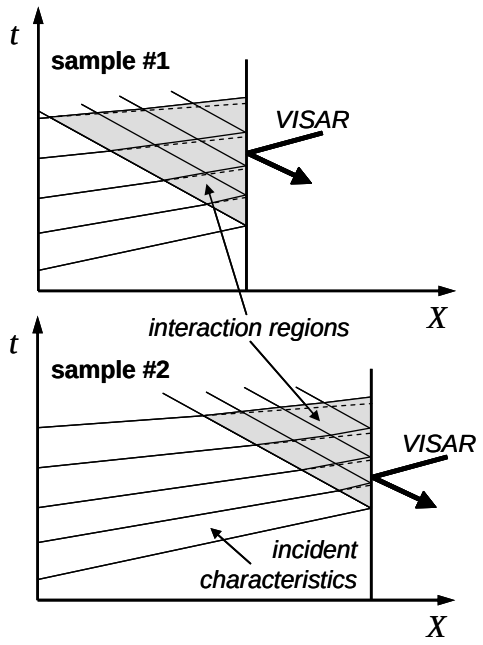

Figure 1. Schematic of ramp-wave experiment using two samples, showing interaction regions (shaded) where incident characteristics are bent by interaction with reflected characteristics. For isentropic flow in semi-infinite samples, incident characteristics would remain straight as shown by the dashed lines.

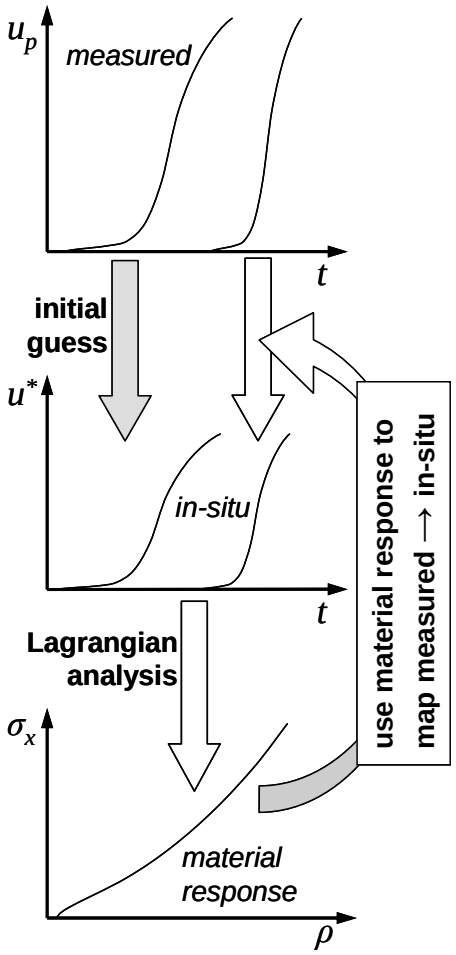

Figure 2. Conceptual diagram of iterative Lagrangian analysis, with an initial guess for the in-situ velocity profiles that would occur at the interface positions for semi-infinite samples. The Lagrangian analysis and mapping steps are repeated until the material response no longer changes.

ity. The latter effect is often referred to as the "bending of characteristics" due to the ramp-wave interaction.

Inverse analysis using iterative Lagrangian analysis postulates the existence of a mapping between the measured interface-velocity history and the in-situ velocity history that would occur at the same position in the absence of any interface. This mapping can be computed as described in Section 2.2, and depends on both the sample material response and the shape of the ramp wave. The material response itself is determined by Lagrangian analysis of the in-situ velocity profiles (assuming simple-wave behavior), thus iteration is required to obtain a result. Starting with an initial guess either for the in-situ velocity profiles or for the material response, the mapping and Lagrangian analysis steps are repeated until the resulting material response no longer changes with further iterations. This iterative procedure is depicted conceptually in Figure 2 for the case of an initial guess for in-situ velocity profiles. To differentiate between particle velocity in the finite-thickness samples and the in-situ particle velocity used to compute material response, the latter is henceforth referred to by the symbol u^*. Under the simple-wave assumption of the Lagrangian analysis step, the in-situ velocity u^* acts as a material state variable; material response can be represented by the single-valued functions $c_L(u^*)$, $\sigma_x(u^*)$, and $v(u^*)$. With $c_L(u^*)$ found by fitting sets of points $[X, t(u^*)]$ to straight lines, Equations (1) become

$$dv = -du^* / \rho_0 c_L(u^*) \qquad \text{and} \qquad d\sigma_x = \rho_0 c_L(u^*) du^*. \tag{2}$$

2.2. Backward Characteristics to Map Measured Profiles to In-Situ

Characteristics are curves in *X-t* along which the partial differential equations of motion reduce to an ordinary differential equation; their slope *dX/dt* at any point is equal to the local Lagrangian speed of propagation, or sound speed, in either the positive or the negative direction. For isentropic flow, the differential equation along a characteristic can be expressed by the Riemann invariants R^+ along positive (*dX/dt > 0*) characteristics and R^- along negative (*dX/dt < 0*) characteristics, where [14]

$$R^{\pm} = u_p \pm F \qquad \text{and} \qquad F = \int d\sigma_x / \rho_0 c_L = u^*. \tag{3}$$

The function F is a material state variable, and the equality $F = u^*$ comes from the second of Equations (2). In a simple-wave region with a right-going compression wave, $u_p = u^*$ and thus $R^+ = 2u_p$ and $R^- = 0$. In a region of non-simple (but still isentropic) flow, such as the wave interaction region near an interface, $u_p \neq u^*$ and $R^{\pm}$ relate the local particle velocity to the local material state. If the Riemann invariants are known from initial or boundary conditions for a particular positive characteristic and a particular negative characteristic, then the particle velocity and material state at the point where these two characteristics intersect is given by Equations (3) as

$$u_p = \frac{R^+ + R^-}{2} \qquad \text{and} \qquad F = u^* = \frac{R^+ - R^-}{2}. \tag{4}$$

The characteristics equations and Riemann invariants are used in a backward calculation to determine the material state along the first negative characteristic emanating from the sample's right boundary, given the time-history of particle velocity and material state on that boundary as well as the material response function $c_L(u^*)$. As shown in Figure 3, this first negative characteristic is the boundary of the interaction region, thus the material state along it completely describes the undisturbed simple-wave region to its left. A mesh of intersecting positive and negative characteristics describes the interaction region, with each intersection referenced by the indices (*ineg*, *ipos*) of the corresponding characteristics.

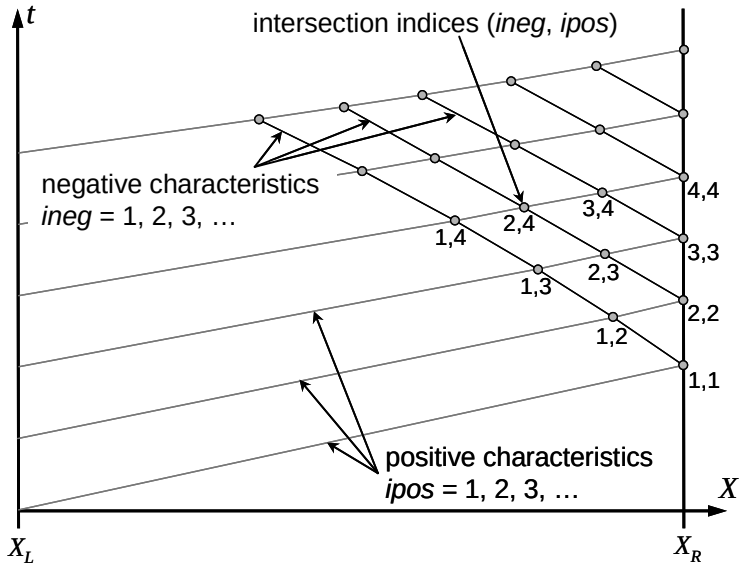

Figure 3. Mesh of intersecting characteristics used for backward determination of the simple-wave region bordered by negative characteristic *ineg* = 1 from the measured velocity history along $X = X_R$.

The particle velocities u_p at intersections where *ipos* = *ineg* on the boundary $X = X_R$ are taken directly from the experimentally measured interface velocity. The longitudinal stresses σ_R at these intersections are then either set identically equal to zero for a free-surface condition, or determined from the known $\sigma_x(u^*)$ function of a window material. The latter requires simple-wave flow in the window adjacent to the interface, so that u^* in the window is equal to u_p at the interface; if a shock forms and grows downstream in the window, this condition will be violated beyond a certain time. Since the material response functions are single-valued, c_L and u^* at the boundary intersections are then determined uniquely by σ_R.

The backward calculation proceeds by computing u_p, u^*, σ_x, c_L, t, and X at each of the intersections (*ineg*, *ipos*) from known values at the intersections (*ineg* + 1, *ipos*) and (*ineg*, *ipos* – 1) as follows:

$$R^+_{ipos} = u_{p(ineg+1,ipos)} + u^*_{(ineg+1,ipos)}, \quad R^-_{ineg} = u_{p(ineg,ipos-1)} + u^*_{(ineg,ipos-1)}; \tag{5}$$

$$u_{p(ineg,ipos)} = \frac{R^+_{ipos} + R^-_{ineg}}{2}, \quad u^*_{(ineg,ipos)} = \frac{R^+_{ipos} - R^-_{ineg}}{2}; \tag{6}$$

$$\sigma_{x(ineg,ipos)} = \sigma_x\left(u^*_{(ineg,ipos)}\right), \quad c_{L(ineg,ipos)} = c_L\left(u^*_{(ineg,ipos)}\right); \tag{7}$$

$$C_{ipos} = \frac{c_{L(ineg,ipos)} + c_{L(ineg+1,ipos)}}{2}, \quad C_{ineg} = \frac{c_{L(ineg,ipos)} + c_{L(ineg,ipos-1)}}{2}; \tag{8}$$

$$t_{(ineg,ipos)} = \frac{X_{(ineg,ipos-1)} - X_{(ineg+1,ipos)} + C_{ineg}t_{(ineg,ipos-1)} + C_{ipos}t_{(ineg+1,ipos)}}{C_{ipos} + C_{ineg}}; \tag{9}$$

$$X_{(ineg,ipos)} = X_{(ineg,ipos-1)} - C_{ineg}\left(t_{(ineg,ipos)} - t_{(ineg,ipos-1)}\right). \tag{10}$$

In Equation (8), the slope of a characteristic between two intersections is approximated by the average of the Lagrangian wave speeds at the two intersections. Equations (9) and (10) are the solution for the intersection of two lines in the *X*-*t* plane, one passing through the point at intersection (*ineg*, *ipos* – 1) with slope C_{ineg}, the other passing through the point at intersection (*ineg* + 1, *ipos*) with slope C_{ipos}. For the example mesh in Figure 3, the calculation would start by computing intersection (1, 2) from the boundary intersections (1, 1) and (2, 2), then intersection (2, 3) from (2, 2) and (3, 3), then intersection (1, 3) from (1, 2) and (2, 3), and so on until all the intersection points on *ineg* = 1 are known.

After the first negative characteristic of the thinnest sample reaches the left boundary at $X = X_L$, the different thickness samples no longer see identical loading histories, violating a necessary condition for the application of Lagrangian analysis. In magnetically driven isentropic compression experiments, magnetic field diffuses into the electrode material, bringing high electrical current with it that joule heats the material to liquid, gas, and plasma states. If this joule heating reaches the sample's left boundary before the first negative characteristic does, or if the sample is the electrode itself, then the condition of identical loading histories for all samples will be violated at an earlier time when the first negative characteristic interacts with the joule-heated material. The time at which this interaction occurs cannot be determined from the characteristics calculation, which completely neglects magnetic diffusion and joule heating. At times prior to this interaction, the backward characteristics solution for material state and velocity is decoupled from the details of how the loading history was generated in the joule-heated region.

With the particle velocity and material state now known at each intersection (1, *ipos*) on the first negative characteristic, the in-situ velocity $u^*(t)$ that would occur at $X = X_R$ for a semi-infinite sample is found simply by projecting the positive characteristics forward as straight lines of slope $c_{L(1,ipos)}$:

$$\left(t_{ipos}\right)_R = t_{(1,ipos)} + \frac{X_R - X_{(1,ipos)}}{c_{L(1,ipos)}}, \quad \left(u^*_{ipos}\right)_R = u^*_{(1,ipos)}. \tag{11}$$

This completes the mapping of a measured interface-velocity history to the corresponding in-situ velocity history for a given material response. As described in Section 2.1, Lagrangian analysis of the in-situ profiles provides an improved estimate of the material response, which can then be used to recompute an improved estimate of the in-situ profiles, and so on in an iterative fashion.

If the window material has higher acoustic impedance than the sample material, the maximum of σ_R will be higher than the maximum in-situ σ_x along *ineg* = 1. Lagrangian analysis gives material response only for in-situ σ_x, thus extrapolation of the material response is required to obtain a backward characteristics solution. Since the extrapolated region is used to compute intersections on positive characteristics connecting in-situ stress states on *ineg* = 1 to higher stress states at $X = X_R$, the method of extrapolation can affect the deduced material response in its non-extrapolated region. Thus, care must be taken to ensure the extrapolation is realistic.

2.3. Propagation of Uncertainties

Experimental uncertainties in velocity and time of the measured interface-velocity histories, and in thickness of the samples, can be propagated through the iterative Lagrangian analysis procedure to give uncertainties in the deduced material response. Time and thickness uncertainties are generally provided as single numbers δt_i and δx_i for each profile *i* (each sample). Velocity uncertainty varies with magnitude of the velocity and is found by combining experimental uncertainties in the velocity-per-fringe of the interferometer (δVPF_i) and in the fringe count of the measurement (δFC_i);

$$\delta u_i(u) = \sqrt{\left(\delta VPF_i \cdot u_i / VPF_i\right)^2 + \left(\delta FC_i \cdot VPF_i\right)^2} \ . \tag{12}$$

For the case of in-situ Lagrangian analysis of *N* profiles $t_i(u)$, uncertainty δc_L at each value of velocity is given simply by the uncertainty in the slope of a linear least-squares fit to a set of $X(t)$ data, with all three sources of uncertainty transferred to the independent variable of the fit using derivatives:

$$\delta T_i(u) = \sqrt{\delta t_i^{\,2} + \left(\frac{\delta u_i}{du/dt_i}\right)^2} \ , \tag{13}$$

$$\delta X_i(u) = \sqrt{\delta x_i^{\,2} + \left(c_L \delta T_i\right)^2} \ . \tag{14}$$

Equation (13) gives the total time uncertainty $\delta T_i(u)$ due to contributions from both time and velocity uncertainties, the latter folded in by the local derivative of the velocity profile. Equation (14) gives the total "thickness" uncertainty $\delta X_i(u)$ due to contributions from the sample thickness uncertainty and the total time uncertainty, the latter folded in by the slope (wave speed) c_L of the fit to $X(t)$. The uncertainty in slope for a least-squares fit is then given by [15]

$$\delta c_L(u) = \sqrt{\frac{\sum \frac{1}{\delta X_i^{\,2}}}{\sum \frac{1}{\delta X_i^{\,2}} \sum \frac{X_i^{\,2}}{\delta X_i^{\,2}} - \left(\sum \frac{X_i}{\delta X_i^{\,2}}\right)^2}} \ . \tag{15}$$

For inverse Lagrangian analysis, however, measurement uncertainties are known for the interface-velocity histories $u_p(t)$, not the in-situ velocity histories $u^*(t)$. Equations (13) through (15) can still be used if $\delta T_i(u_p)$ can be mapped, even approximately, to $\delta T_i(u^*)$. Each value of u_p at the measurement

interface corresponds to a value of u^* at the same position by the backward computation (through the interaction region) and forward projection (for the in-situ case) of a positive characteristic. The bending of characteristics in the interaction region tends to locally either bunch together or spread out the arrival times for particular values of u^* relative to the corresponding values of u_p (see Figure 1). Thus $\delta T_i(u^*)$ can be approximated by assuming that the relative change in local spacing Δt of the time grid when transforming from measured to in-situ velocity histories also applies to the time uncertainties:

$$\delta T_i(u^*) = \frac{\Delta t_{u^*(t)}}{\Delta t_{u_p(t)}} \delta T_i(u_p). \tag{16}$$

The local spacing at a particular time point is defined as the average of the forward and backward differences from that point.

Once $\delta c_L(u^*)$ is known, the upper and lower uncertainty bounds for longitudinal stress and density are found by integrating Equations (2) with $c_L(u^*)$ replaced by $c_L(u^*) \pm \delta c_L(u^*)$.

The procedure outlined above in Equations (12) through (16) constitutes the first of three different options provided by CHARICE for computing uncertainties. The second option follows a very similar procedure, except that experimental time uncertainties are not used. Instead, the in-situ time uncertainty is estimated as a function of velocity from the first negative (backward-computed) characteristics. For each sample, the first negative characteristic is projected to the position of the thinnest sample's back surface, $X_{Rmin} = \min(X_i)$. The resulting curves of in-situ velocity at X_{Rmin} are interpolated onto a common u^* grid, and $\delta t_i(u^*)$ is given at each value of u^* as the deviation in time of curve i from the average time of all the curves at that u^*. Since time uncertainty is defined for the in-situ case, the time-spacing conversion in Equation (16) applies only to the measured velocity uncertainty. Thus, Equations (13) and (16) are replaced by

$$\delta T_i(u^*) = \sqrt{\delta t_i^{\,2}(u^*) + \left(\frac{\Delta t_{u^*(t)}}{\Delta t_{u_p(t)}} \cdot \frac{\delta u_i}{(du_p/dt)_i} \right)^2}\ . \tag{17}$$

This second method for computing uncertainties essentially computes the time uncertainties from the scatter in the data, instead of using fixed experimental timing uncertainties. This may be useful in cases where experimental time uncertainties are not available or include significant correlated systematic error.

The third option for computing uncertainties in CHARICE follows a brute-force approach not related to the first two methods. For each uncertainty δt_i, δx_i, and $\delta u_i(u_p)$ of each measured interface-velocity profile, a new iterative Lagrangian analysis is performed with the appropriate input data perturbed in the positive direction to obtain a corresponding perturbed $c_L(u^*)$ curve. For a problem with N velocity profiles, this requires $3N$ full computations, but each computation can use the nominal result (without perturbation) as the initial guess. Assuming that c_L varies linearly with small perturbations to the inputs, each computation gives the sensitivity of c_L to changes in particular input data; for example, $\partial c_L/\partial x_i = [c_L(x_i + \delta x_i) - c_L(x_i)]/\ \delta x_i$. The final uncertainty $\delta c_L(u^*)$ is then simply given by adding all the sensitivities in quadrature:

$$\delta c_L(u^*) = \sqrt{\sum \left(\delta x_i \frac{\partial c_L}{\partial x_i} \right)^2 + \sum \left(\delta t_i \frac{\partial c_L}{\partial t_i} \right)^2 + \sum \left(\delta u_i \frac{\partial c_L}{\partial u_i} \right)^2}\ . \tag{18}$$

This third method is the most rigorous for uncorrelated errors, but requires significant computational time.

The three methods for computing uncertainties can be summarized as follows:

1. use experimental time uncertainties, translate time + velocity uncertainties to in-situ case;

2. obtain in-situ time uncertainties from spread in backward-projected profiles, translate velocity uncertainties to in-situ case;

3. compute linear sensitivities to time, velocity, and thickness uncertainties.

2.4. Correction for Unequal Baseplate Thicknesses

The iterative Lagrangian technique for inverse analysis requires that all the samples see identical loading histories. Experimentally this is ensured by mounting all the samples on a baseplate that is driven uniformly; for magnetically driven ramp waves, the baseplate is an electrode exposed to a uniform magnetic field history. Manufacturing tolerances, however, can cause the baseplate to have a slightly different thickness behind each sample, so that even if the baseplate is loaded uniformly, each sample will see a slightly different loading history due to the longer or shorter propagation distance in the baseplate. Since this causes only small changes to the time of arrival of each stress level at the sample, it can approximately be corrected for if the response of the baseplate material is known.

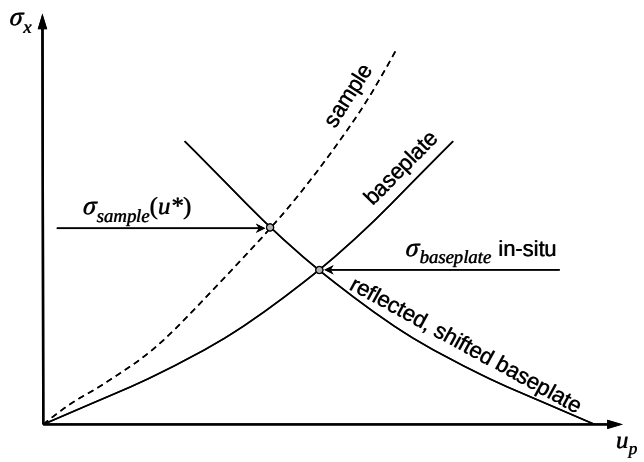

Figure 4. Impedance matching of in-situ stress in the sample, corresponding to a particular value of in-situ velocity u^*, to in-situ stress in the baseplate, used to determine timing corrections for unequal baseplate thicknesses.

The correction for an off-nominal baseplate thickness is applied to the in-situ velocity profile at X_R after it has been computed from the measured in-situ velocity profile, but before applying the Lagrangian analysis step. For each point in $u^*(t)$, the time is adjusted by the difference from nominal propagation time in the baseplate at the corresponding in-situ stress level in the baseplate:

$$\delta t_{baseplate} = \frac{\delta x_b}{c_L(\sigma_{baseplate})}, \tag{19}$$

where δx_b is the difference from nominal baseplate thickness for a particular sample, $c_L(\sigma_{baseplate})$ is the material response function of the baseplate material, and $\sigma_{baseplate}$ is found from the corresponding value of $\sigma_{sample}(u^*)$ by impedance matching in the σ-u_p plane as shown in Figure 4.

For each point in $u^*(t)$, σ_{sample} is found from the sample response function. The baseplate response function $\sigma_{baseplate}(u^*)$ is reflected and shifted to intersect the sample response function at σ_{sample}. Then the in-situ $\sigma_{baseplate}$ is given by the intersection of the original and reflected/shifted baseplate response curves. Finally, $c_L(\sigma_{baseplate})$ is found from the baseplate response function. This approach accounts

for the mismatch in acoustic impedance between the baseplate and sample materials, but neglects the bending of characteristics in the interaction region upstream of the baseplate/sample interface. Since the deviations in baseplate thickness are small, the interaction region would be approximately the same size for all samples, and thus the effect of bending characteristics should cancel out to first order. The example in Section 5.3 demonstrates this technique.

3. Setup GUI

CHARICE uses a Setup GUI, shown in Figure 5, to aid the user in setting up a problem for analysis. Most of the interface consists of an input form where values for all the parameters needed to run a calculation may be set. The upper right panel is a plot of the measured interface-velocity profiles currently loaded, and underneath this is a row of action buttons. A bar at the bottom displays help messages upon mouse rollover of any active element.

The general procedure for setting up a problem begins by first using the *UFILES* parameter to load experimental interface-velocity profiles. Then the *TMIN*, *UMIN*, and *UMAX* parameters are used to truncate each profile to the desired velocity range to be used in the analysis, while the *SGDEG* and *SGWIN* parameters are used to apply filtering if desired. The time and velocity of the original profiles may be scaled to the desired units at any time during setup. Finally, remaining needed parameters are set, such as: general settings (Section 3.1); sample thickness, time shifts, and uncertainties (Section 3.2); equation-of-state (EOS)* input for other materials in the problem (Section 3.3); and

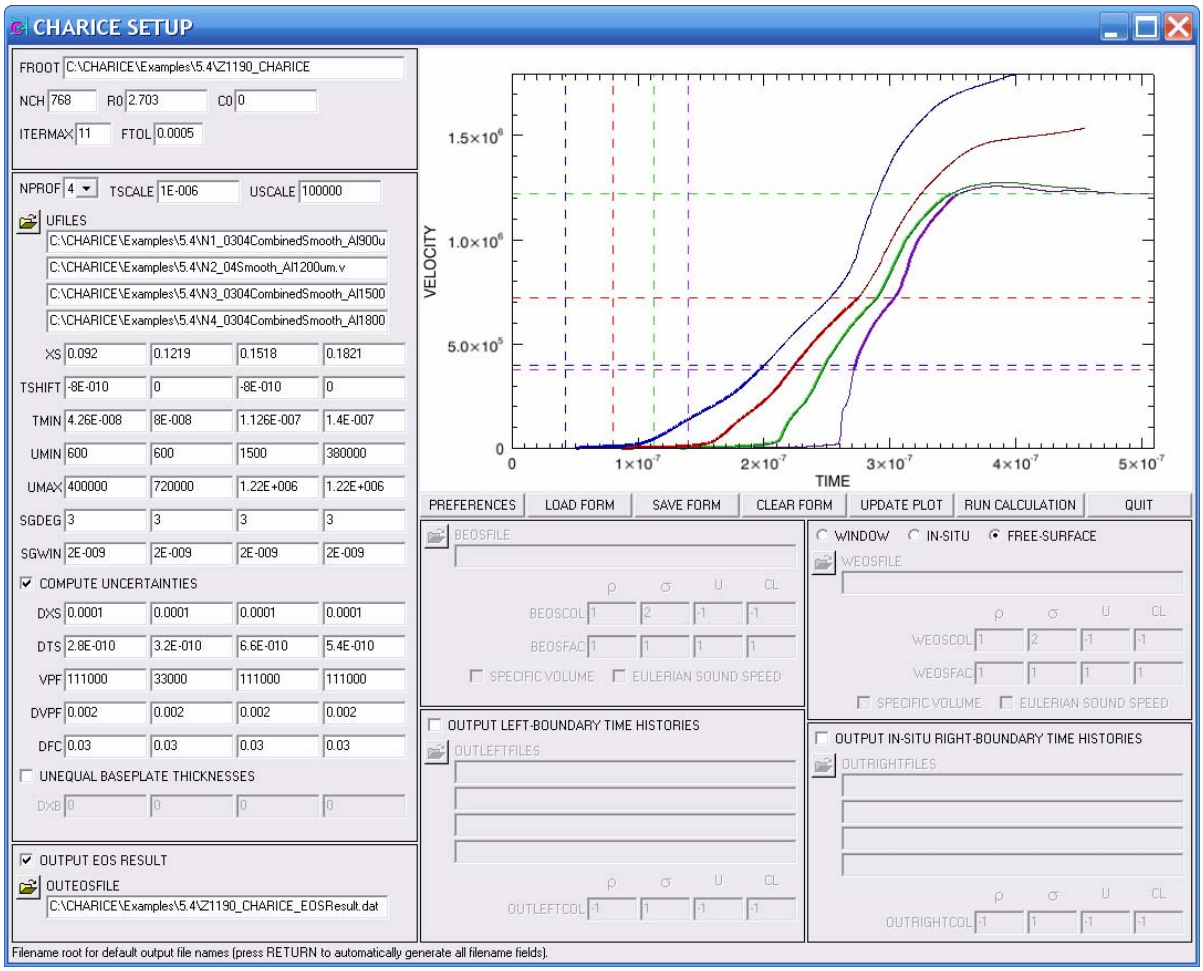

Figure 5. Setup GUI of CHARICE under Windows XP, with parameters set for the example problem of Section 5.4. All of the input-form parameters are listed in Appendix B with short descriptions, and explained more thoroughly in Sections 3.1–3.4.

* For reasons of brevity, the term EOS is often used subsequently in this report to mean a material's mechanical compression response. It must be emphasized that this "material response" is not a complete equation of state.

output control (Section 3.4). Appendix B provides a more compact list of the input parameters with short descriptions. Section 3.5 details the procedure used by CHARICE to process the input velocity profiles using data from the input form.

Input form data can be saved to and loaded from files using the SAVE FORM and LOAD FORM buttons. These setup files are in ASCII format and may be edited or even created offline by the user; the file specification is given in Appendix B. Pressing SAVE FORM will display an error if the form data are not complete enough to run a calculation. All data presently on the form can be erased by pressing CLEAR FORM. Units for data in the form are arbitrary but must be self-consistent. Although displayed with absolute paths in the Setup GUI, filenames are converted to relative paths when writing them to the setup form file. This allows a setup form file to continue to work correctly if the associated external input files are moved with it to another location in the file system.

The PREFERENCES button brings up a modal dialog box where global preferences can be set; these include certain default parameter values, warnings that can be turned on or off, graphics settings, and the preferred numerical precision for calculations. See Appendix A for details. Preference settings are automatically saved to a file upon exiting CHARICE, and automatically reloaded the next time CHARICE is launched.

The plot shows raw measured interface-velocity profiles (input from files) as thin, dark solid curves, and the processed (filtered and truncated to the desired velocity range) velocity profiles as thick, bright solid curves. Dashed lines indicate the velocity and time limits used to process the data. Lines and curves are color coded by profile number, with nine colors available in the order blue, red, green, purple, cyan, magenta, yellow, brown, and blue-grey. No legend is provided, as it should be clear from the sample thicknesses which curve corresponds to which profile. To zoom into a region of the plot, CLICK and DRAG a rubber-band box. A warning is displayed if the zoom range is too small to be represented by the tick labels. DOUBLE-CLICK anywhere in the plot to zoom back out to the full extent of the data. The UPDATE PLOT button reprocesses the input velocity profiles using the current form data, setting defaults for certain fields if they are missing values, and redraws the plot using the current zoom ranges.

The RUN CALCULATION button checks the form data for completeness, reprocesses the input velocity profiles, and brings up the CALCULATION GUI discussed in Section 4. The QUIT button exits CHARICE, closing all windows.

The minimum screen size required to view the entire Setup GUI depends on the number of profiles used in a problem. With four profiles as shown in Figure 5, the minimum standard screen size is 1280 × 854 pixels under Windows XP systems and 1400 × 1050 pixels under UNIX-based systems.

3.1. General Settings

Following are descriptions of the global parameters found in the general settings section of the input form in the upper left corner of the GUI.

FROOT: The path and base filename for all output files. Pressing RETURN in this field automatically sets all output filenames on the form using default name endings set in the preferences. Unless they have been changed, these are "*FROOT*_EOSResult.dat" for the EOS results output, "*FROOT_sample#*_LeftBoundary.dat" for the left-boundary time histories, and "*FROOT_sample#*_InterfaceInSitu.dat" for the right-boundary in-situ time histories. Upon loading an input file missing the *FROOT* parameter, it is defaulted to the path and base of the input filename.

NCH: The number of characteristics or points to use in the calculations. For measured interface-velocity profiles, characteristics are distributed on a uniform time grid across the velocity range used in the backward calculation. In order to compute $c_L(u^*)$, in-situ velocity profiles are re-interpolated onto a uniform velocity grid of *NCH* points. If not set, *NCH* defaults to the smallest number of points encompassed by the desired velocity range in the original measured velocity files. Pressing RETURN updates the velocity profiles plot (the time resolution of the processed profiles depends on *NCH*).

R0: The ambient density ρ_0 of the sample material, a required parameter.

C0: The ambient sound speed c_0 of the sample material, required when using an interferometer window in order to set the first guess for in-situ velocity histories from the ambient impedance mismatch. If set, regardless of whether a window is used, the value of *C0* will be pre-pended to c_L results at $u^* = 0$; otherwise, the value of c_L at $u^* = 0$ is copied from the first point at $u^* > 0$.

ITERMAX: The maximum number of iterations to perform in the calculation; if $c_L(u^*)$ has not converged after *ITERMAX* iterations of the measured-to-in-situ mapping and Lagrangian analysis steps, the calculation stops anyway. The default value of *ITERMAX* is 6 and can be changed in preferences.

FTOL: Tolerance in the mean root square of the fractional deviation of $c_L(u^*)$ from the previous iteration, defined by Equation (21), below which the calculation stops and $c_L(u^*)$ is considered to be converged. The default value of *FTOL* is 0.001 and can be changed in preferences.

3.2. Velocity Profile Settings

Below the section of general settings is a large section of parameters pertaining to the measured velocity profiles. Most of these are array-based parameters requiring a separate value for each profile (each sample) in the problem. Where it makes sense to, the values for profiles #2 and up may be copied from the value for profile #1 by RIGHT-CLICKING on any of the fields for that parameter and selecting the pop-up menu item "Duplicate First Field." If a parameter can affect the processing of input velocity profiles, then pressing RETURN in any of the fields for that parameter updates the plot of velocity profiles, but does not set defaults for other missing parameters as pressing the UPDATE PLOT button does. Following are descriptions of the individual parameters and switches.

NPROF: A drop-down list to select the number of profiles (samples) in the problem. The calculation requires at least two profiles, and the maximum number of profiles allowed can be set in preferences (the default is 5 unless this has been changed). Upon changing the number of profiles, the Setup GUI changes to show the correct number of fields for array-based parameters; data in the last profile(s) are lost when the number of profiles is reduced.

TSCALE: A time scale factor applied to all the original (raw) input velocity profiles. Pressing RETURN in this field also applies the scale factor to the *TSHIFT*, *TMIN*, *SGWIN*, and *DTS* parameters, accounting for any previously applied scale factor, and updates the velocity plot. The default is 1.

USCALE: A velocity scale factor applied to all the original (raw) input velocity profiles. Pressing RETURN in this field also applies the scale factor to the *UMIN*, *UMAX*, and *VPF* parameters, accounting for any previously applied scale factor, and updates the velocity plot. The default value is 1.

UFILES: The full path and filename from which to load each raw input velocity profile, required to run a calculation. These must be ASCII files with at least two columns (time in the first column and velocity in the second column) and any length header that has at least one non-numeric character in each line. Pressing the open-file icon brings up a dialog box to select the files. Multiple files can be selected if they all reside in the same directory; these are placed in *UFILES* fields in the operating

system's sorting order. Using the file selection dialog or pressing RETURN in one of the fields updates the velocity plot with the new data.

XS: The thickness x_i of each sample, a required parameter.

TSHIFT: A time shift applied individually to each raw input velocity profile, optional (defaults to 0).

TMIN: The minimum time to use when defining the velocity range for each profile; points $t < TMIN$ are discarded prior to searching for the desired minimum velocity point *UMIN*. This can be useful for noisy data when trying to set *UMIN* close to 0. If not set, *TMIN* defaults to the first point of each raw input velocity profile.

UMIN: The minimum velocity, or lower endpoint, of the desired velocity range to use for each profile during Lagrangian analysis. (Backward calculations use only the smallest *UMIN* for all profiles.) Typically, this is set as close to 0 as possible, and is the same for all profiles, but may be set differently for a profile to exclude that profile from the calculation below a certain velocity (see example in Figure 5). At least two of the profiles must be set to the smallest value of *UMIN*, because at least two profiles are need in a velocity range to perform an iterative Lagrangian analysis. If not set, *UMIN* defaults to the first point of contiguous, positive increasing velocity in each raw input velocity profile.

UMAX: The maximum velocity, or upper endpoint, of the desired velocity range to use for each profile during both backward calculations and Lagrangian analysis. At least two of the profiles must be set to the largest value of *UMAX*, because at least two profiles are needed in a velocity range to perform an iterative Lagrangian analysis. When processing the input profiles, CHARICE will automatically adjust *UMAX* if needed to meet this condition. Additional profiles may use lower values of *UMAX* to exclude, for example, regions of the velocity profiles that have been contaminated by reverberations in the sample. If not set at all, *UMAX* defaults to the maximum velocity in each raw input velocity profile.

SGDEG: The degree of Savitsky-Golay filtering[16] applied to each raw input velocity profile. This is a digital filter in the time domain that is equivalent to a moving window where the value at the center of the window is replaced by the value at that time of a polynomial least-squares fit to all the points within the window. The polynomial is of degree *SGDEG*. For the same window size, this filter preserves second-derivative information (steep variations) better than simple moving window averages. Good values for *SGDEG* are typically 3 or 4. If set to 0 (the default), the corresponding profile is not filtered.

SGWIN: The window size, in time units, for Savitsky-Golay filtering of each raw input velocity profile. Filtering uses a symmetric window. *SGWIN* must encompass at least *SGDEG* points of the input velocity profile. When processing the input profiles, CHARICE will automatically adjust *SGWIN* if needed to meet this condition. If not set, *SGWIN* defaults to 2% of the time range of the input profiles. The *SGWIN* fields are not active unless there is at least one non-zero value in the *SGDEG* fields.

COMPUTE UNCERTAINTIES: Check this box to activate the following five parameters and allow uncertainty propagation to be calculated later in the Calculation GUI, as described in Section 2.3.

DXS: The absolute experimental uncertainty δx_i in sample thickness for each profile, defaults to 0.

DTS: The absolute experimental uncertainty δt_i in time for each profile, defaults to 0.

VPF: The velocity-per-fringe of the interferometer for each profile. Entries here are required when computing uncertainties, because the "default" value of 0 is invalid.

DVPF: The fractional (not absolute) uncertainty in *VPF*, defined as $\delta VPF/VPF$. The default value of 0.002 may be changed in preferences.

DFC: The absolute uncertainty δFC in fringe count for each profile. The default value of 0.02 may be changed in preferences.

UNEQUAL BASEPLATE THICKNESSES: Check this box to activate the following parameter as well as the baseplate EOS input section, and specify that the calculation include corrections for unequal baseplate thicknesses as described in Section 2.4.

DXB: The deviation δx_b of the thickness for each sample's baseplate from the nominal baseplate thickness, defaults to 0.

3.3. Input EOS Settings

The two sections of the input form just underneath the row of action buttons (see Figure 5) are used to specify settings for input of ramp-wave material response, or EOS, for the baseplate and window materials. Each section is only active if needed. The input control parameters allow the user to read any column-formatted ASCII file that has data for at least two of the four variables ρ (or v), σ_x, u^*, and c_L (or Eulerian wave speed c), regardless of which columns they are in or what units they use. Thus, the user generally has no need to pre-process output from other programs used to generate material response curves, including CHARICE itself. Following are descriptions of the individual parameters.

BEOSFILE: The full path and filename from which to load the baseplate EOS. This must be a column-formatted ASCII file with two or more columns and any length header that has at least one non-numeric character in each line. At least 2, but as many as 4 of the columns must contain data from 2-4 of the following variables: density (or alternately specific volume), longitudinal stress, velocity, and Lagrangian wave speed (or alternately Eulerian wave speed). The columns may be in any order, and may be mixed in with other unused columns. Pressing the open-file icon brings up a dialog box to select the file.

BEOSCOL: This array of fields, one for each of the four possible variables to be input, specifies which column in *BEOSFILE* holds a particular variable. The column numbering starts at 1, and a field set to -1 indicates that the corresponding variable is not available in *BEOSFILE* and will not be loaded. The default arrangement is density in the first column and stress in the second column.

BEOSFAC: This array of fields, one for each of the four possible variables to be input, specifies a scale factor to be applied to each variable as it is read from the file. The default is 1.

SPECIFIC VOLUME: Check this box to specify that specific volume will be read from *BEOSFILE* instead of density. The corresponding label above the *BEOSCOL* array changes as a reminder.

EULERIAN SOUND SPEED: Check this box to specify that Eulerian wave speed will be read from *BEOSFILE* instead of Lagrangian wave speed. The corresponding label above the *BEOSCOL* array changes as a reminder.

WINDOW / IN-SITU / FREE-SURFACE: This set of exclusive buttons is used to select the boundary condition at the measurement interface. The default is *FREE-SURFACE* (zero stress). Selecting *WINDOW* activates the window EOS input section below. If *IN-SITU* is selected, then the calculation will consist of a single Lagrangian analysis of the measured profiles.

WEOSFILE, WEOSCOL, WEOSFAC, etc.: Each of these parameters in the window EOS input section all behave in exactly the same fashion as the corresponding parameter in the baseplate EOS input section described above, but apply to the window EOS.

3.4. Output File Settings

The three sections along the bottom edge of the Setup GUI control file output of results from an iterative Lagrangian analysis. Following are descriptions of the individual parameters.

OUTPUT EOS RESULT: This box is checked by default to request file output of the EOS result for the sample material. Uncheck it if this output is not desired.

OUTEOSFILE: The full path and filename for writing the EOS result. The file created is a fixed-width, column-formatted ASCII file with a single-line header giving the column names. The columns are 15 characters wide. If uncertainties were not computed, the file has four columns in the order u^*, c_L, ρ, σ_x. If uncertainties were computed, the file has nine columns in the order u^*, c_L, δc_L, ρ, σ_x, ρ_{LOW}, σ_{LOW}, ρ_{HIGH}, σ_{HIGH}, where the subscripts *LOW* and *HIGH* refer to lower and upper uncertainty bounds for density and longitudinal stress. The data are written in exponential notation with seven significant digits.

OUTPUT LEFT-BOUNDARY TIME HISTORIES: Check this box to request file output of the time history of certain variables at the left boundary of each sample. These are found by projecting points on the first (undisturbed) negative characteristic, from the current iteration of the analysis (see Section 4), to $X = X_L$ for each sample. Where the sample material response exhibits a localized region of $\partial c_L/\partial u^* < 0$, such as at a transition from elastic to plastic compression, it is common to find the projected incident characteristics crossing each other, which causes a glitch in the left-boundary time history (CHARICE deletes projected characteristics that cross previously-determined characteristics). This phenomenon is due to discretization of the material response and/or small uncertainties in the experimental velocity data such as noise or slightly different material response from sample to sample.

OUTLEFTFILES: The full path and filename for the left-boundary time history of each sample. Pressing the open-file icon brings up a dialog to select the directory for these files; individual filenames must then be entered manually. Alternatively, pressing RETURN in the *FROOT* field fills the *OUTLEFTFILES* fields automatically using the value of *FROOT* with default filename endings. The files created are fixed-width, column-formatted ASCII files with a single-line header giving the column names. The columns are 15 characters wide. The file has 2-5 columns, with time in the first column, and subsequent columns defined by the parameter *OUTLEFTCOL*. The data are written in exponential notation with seven significant digits.

OUTLEFTCOL: This array of fields, one for each of the four possible output variables, specifies which column to the right of the time column holds a particular variable. Column number 1 refers to the first non-time column, or the second column in the file. A field set to -1 indicates that the corresponding variable will not be written to the file. The default arrangement is longitudinal stress in the first non-time column, with no other variables output.

OUTPUT IN-SITU RIGHT-BOUNDARY TIME HISTORIES: Check this box to request file output of the time history of certain variables at the measurement interface position for the in-situ (semi-infinite sample) case of each sample. These are found from the in-situ velocity profiles $u^*(t)$ used for Lagrangian analysis in the current iteration of the analysis (see Section 4).

OUTRIGHTFILES, OUTRIGHTCOL: These two parameters behave in exactly the same fashion as the *OUTLEFTFILES* and *OUTLEFTCOL* parameters described above for output of left-boundary time histories, but apply to the in-situ right-boundary time history output files.

3.5. Processing of Velocity Profiles

The routines that process the input velocity profiles (after pressing RETURN in certain fields, pressing UPDATE PLOT, or pressing RUN CALCULATION) for use in the calculation perform the following sequence of operations.

1. Load velocity profiles from individual files, applying *TSCALE* and *USCALE*.
2. Shift the time data for each profile by the corresponding value of *TSHIFT*.
3. If *TMIN* for any profile is out of the (now shifted) time data range, or is not provided, set it to the default value (first point of time data).
4. Using the parameters *SGDEG* and *SGWIN*, apply a Savitsky-Golay digital filter to each profile, using default values (*SGDEG* = 0, *SGWIN* = 2% of time range) for missing parameters.
5. If *UMIN* for any profile is out of the (now filtered) velocity data range, or is not provided, set it to the default value (first point of contiguous positive increasing velocity).
6. If *UMAX* for any profile is out of the (now filtered) velocity data range, or is not provided, set it to the default value (maximum velocity).
7. If the smallest *UMIN* or largest *UMAX* occurs at only one profile, set its value identical to the second-smallest *UMIN* or second-largest *UMAX* to ensure at least two profiles are included at the endpoints of the largest range of velocity.
8. For each profile, look on $t \geq TMIN$ to find the first point where $u_p \geq \min(UMIN)$ and interpolate to find the exact time endpoint t_{UMIN} that corresponds to min(*UMIN*).
9. For each profile, find the first point where $u_p \geq UMAX$ and interpolate to find the exact time endpoint t_{UMAX} that corresponds to *UMAX*.
10. If *NCH* is not provided, set it to the default value (smallest number of points between t_{UMIN} and t_{UMAX} among input profiles).
11. Set up a new uniform time grid array for each profile with $NCH \times (t_{UMAX} - t_{UMIN}) / \max(t_{UMAX} - t_{UMIN})$ points going from t_{UMIN} to t_{UMAX}, and interpolate corresponding velocity arrays from the original input profiles, forcing first and last points to exactly min(*UMIN*) and *UMAX*.
12. Define index pointers to elements of new arrays closest to *UMIN* and *UMAX* for each profile.

Note that the processed velocity profiles all start at min(*UMIN*), but each profile maintains a pointer to its individual *UMIN* point, which will be carried through to the Lagrangian analysis step.

This page intentionally left blank.

4. Calculation GUI

Upon pressing the RUN CALCULATION button in the Setup GUI (with a complete input form), the Calculation GUI, shown in Figure 6, appears in a new window. This interface allows the user to control the inverse Lagrangian calculation as well as view and save results. Multiple simultaneous instances of the Calculation GUI may be opened from the Setup GUI, each with different problem settings. Most of the window is taken up by two plots of the sample material response; the top plot shows $c_L(u^*)$, and the bottom plot shows $\sigma_x(\rho)$. Below the plots is a row of action buttons, and below the buttons is a row of three panels. The left panel displays iteration status, the middle panel controls filtering of the material response, and the right panel selects the method for computing uncertainties. At the bottom of the window is a help bar that displays a message upon mouse rollover of any active GUI element. The minimum standard screen size required to view the entire Calculation GUI under either Windows XP or UNIX-based systems is 1152 × 768 pixels.

The calculation proceeds by numbered "iterations." A single iteration consists of the two steps of first mapping measured interface velocities to in-situ velocities at the interface positions (for all

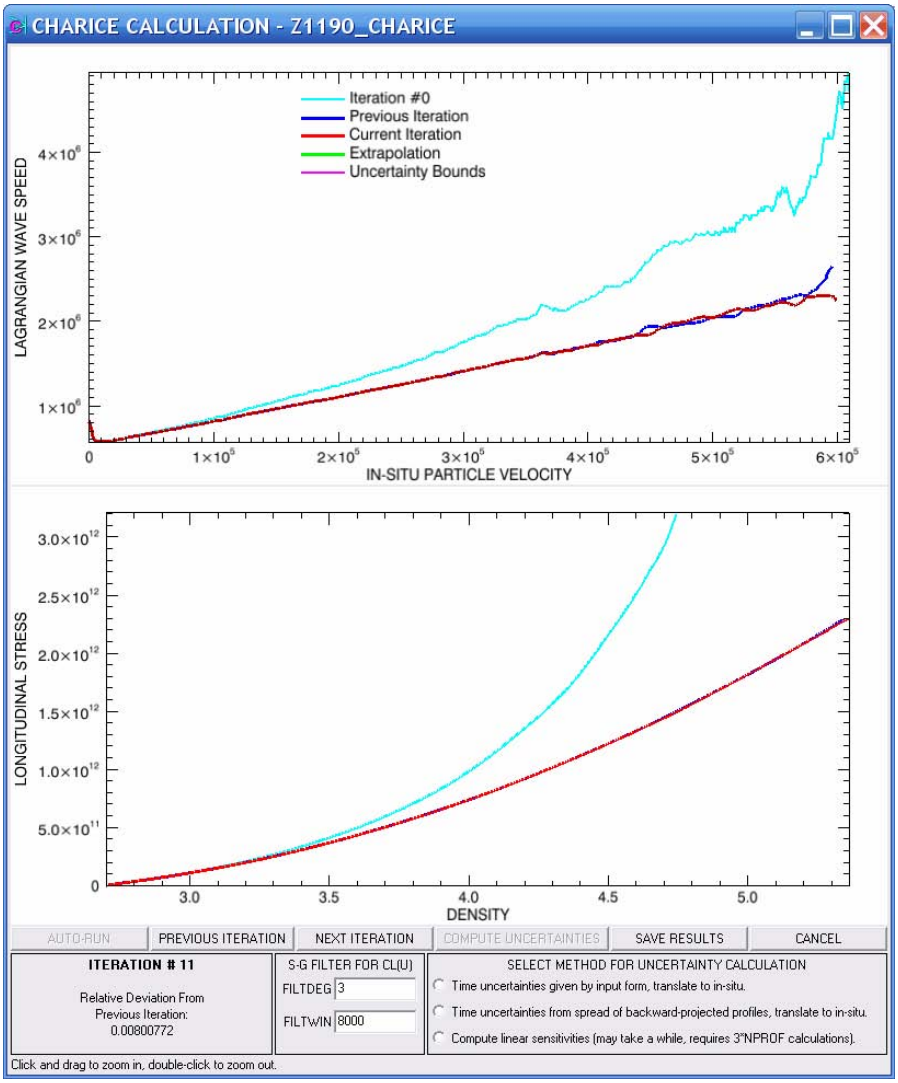

Figure 6. Calculation GUI of CHARICE under Windows XP, showing example problem of Section 5.4.

NPROF samples), then performing Lagrangian analysis on the new in-situ velocity profiles to obtain new EOS curves. The mapping step uses the EOS from the previous iteration. The new EOS is considered the result of the current iteration. The first guess for in-situ velocity profiles and resulting EOS constitute iteration #0. Pressing the AUTO-RUN button runs the calculation until one of the stopping criteria is met; either that the iteration number is equal to *ITERMAX*, or that the mean root square of the fractional deviation of $c_L(u^*)$ from the previous iteration,

$$\text{relative deviation} = \text{mean}\left\langle \sqrt{\left(c_L^{new} - c_L^{old}\right)^2} \Big/ c_L^{old} \right\rangle \tag{20}$$

(the relative deviation displayed in the left panel), is less than or equal to *FTOL*. The PREVIOUS ITERATION and NEXT ITERATION buttons step through the results one iteration at a time, with NEXT ITERATION performing a calculation if needed. The *NEXT ITERATION* button can also be used to continue the calculation beyond the final iteration reached by *AUTO-RUN*.

After any iteration, the filter parameters FILTDEG and FILTWIN in the center panel may be set to smooth the $c_L(u^*)$ curve for that iteration using a Savitsky-Golay digital filter (see Section 3.2). The filtered $c_L(u^*)$ is used to compute $\sigma_x(\rho)$ for the current iteration, which is then used during the mapping step of the next iteration. Press RETURN in either of the two fields to apply the filter parameters. Each iteration may use different filter parameters, but by default they are copied from the previous iteration. The default for iteration #0 is FILTDEG = 0 (no filtering) and FILTWIN = 2% of the velocity range. If the filter parameters for a particular iteration are changed after subsequent iterations have already been computed, then pressing the NEXT ITERATION or AUTO-RUN buttons will recompute the subsequent iterations.

Selecting one of the three methods for computing uncertainties (see Section 2.3) in the right panel activates the COMPUTE UNCERTAINTIES button, which may be pressed after any iteration to compute and plot uncertainty bounds for that iteration. Pressing the SAVE RESULTS button writes output files of the results according to the output control parameters on the Setup GUI (see Section 3.4), then closes the Calculation GUI. Note that if extrapolation of the material response was required during the calculation, the output data encompasses only the non-extrapolated part of the material response. Pressing CANCEL closes the Calculation GUI without saving anything.

The plots display curves for the first-guess iteration #0 (cyan), the previous iteration (blue), and the current iteration (red), as well as the uncertainty bounds (magenta) if they have been computed for the current iteration, and any extrapolation of the material response (green) beyond the maximum in-situ stress needed to encompass the maximum stress level at the interface. CLICK and DRAG a rubberband box to zoom into a region on one of the plots; DOUBLE-CLICK on either plot to zoom out to the full extent of the data. The AUTO-RUN button zooms out after each iteration computed, but the PREVIOUS ITERATION and NEXT ITERATION buttons maintain the current zoom ranges.

4.1. Initialization

When the Calculation GUI first appears, it shows the results for iteration #0, found from Lagrangian analysis of the first guess for in-situ velocity profiles. For a free-surface condition, the first guess in-situ velocity is simply $u^* = u_p/2$. If there are windows on the samples, the first guess in-situ velocity is given by the mismatch in ambient acoustic impedance between the sample and window materials:

$$u^* = \left[\frac{(\rho_0 c_0)_{window} + (\rho_0 c_0)_{sample}}{2(\rho_0 c_0)_{sample}} \right] u_p . \tag{21}$$

This approximates the sample and window EOS curves by straight lines in σ_x-u^* space and neglects the bending of characteristics in the interaction region. It also requires the user to supply the ambient sound speed c_0 of the sample material; if c_0 is not provided, then the first guess is taken as $u^* = u_p$. For the in-situ case, $u^* = u_p$ and the EOS result for iteration #0 is also the final result (no iteration is allowed) unless a correction for unequal baseplates is needed. In the latter case, iterations are allowed but do not include the backward-characteristics mapping step.

If windows are present, then initialization also computes the longitudinal stress σ_R at the sample/window interface corresponding to each point in each profile by assuming simple-wave conditions in the window and interpolating the window EOS curve $\sigma_x(u^*)$ onto u_p. For a free surface condition, σ_R is set equal to 0.

4.2. Calculation Procedure for One Iteration

A single iteration of first mapping measured to in-situ velocity profiles, then performing Lagrangian analysis, adheres to the following sequence of operations.

1. For each profile, find the material state at points on the first negative characteristic corresponding to the points (of uniform spacing in t) in the processed measured velocity array $u_p(t)$ of that profile.

    a. Initialize the intersections along $X = X_R$ with values from $u_p(t)$ and $\sigma_R\ (t)$, with $c_L(t)$ and $F(t)$ found by interpolation from the sample EOS curves.

    b. Use Equations (5)–(10) to determine the material state and velocity at each intersection of characteristics in the interaction region.

    c. If a computed characteristics intersection violates causality (*i.e.*, if $t_{ineg,ipos}$ is not between $t_{ineg+1\ ipos}$ and $t_{ineg\ ipos-1}$, or $X_{ineg,ipos}$ is not less than both $X_{ineg-1,ipos}$ and $X_{ineg,ipos-1}$), then delete one of the characteristics through that intersection based on the values of $\Delta X_{pos} = |X_{ineg+1,ipos} - X_{ineg+1,ipos-1}|$ and $\Delta X_{neg} = |X_{ineg+1,ipos-1} - X_{ineg,ipos-1}|$, *i.e.*, which set of characteristics are spaced closer together.

        i. If $\Delta X_{neg} < \Delta X_{pos}$, delete the current negative characteristic (unless *ineg* = 1, in which case delete the 2nd negative characteristic) and the corresponding positive characteristic that intersects it at $X = X_R$.

        ii. If $\Delta X_{neg} \geq \Delta X_{pos}$, delete the current positive characteristic and the corresponding negative characteristic that intersects it at $X = X_R$.

        iii. If the total number of either positive or negative characteristics deleted, or "merged," exceeds the threshold *WARNTHRESH* set in preferences, display a warning (unless turned off in preferences).

    d. If the computed value of $X_{ineg,ipos} < X_L$, then find where the first negative characteristic intersects X_L, set the material state at that point by interpolation (if *ineg* = 1) or extrapolation (if *ineg* > 1), and recompute the intersections along the current positive characteristic from this point to $X = X_R$; the current positive characteristic becomes the final positive characteristic, the calculation stops, and (unless turned off in preferences) a warning is displayed that the left boundary was reached.

e. Compute density at the points along the first negative characteristic by interpolating from the sample EOS.

2. For each sample, project the points of the first negative characteristic forward to $X = X_R$ to obtain the in-situ velocity profiles $u^*(t)$ according to Equation (11); the resulting arrays will in general have non-uniform spacing in both t and u^*.

    a. If a projected characteristic crosses the previous one ($t_{ipos} \leq t_{ipos-1}$), then delete that characteristic from the result.

    b. If the total number of projected positive characteristics deleted, or "merged," exceeds the threshold *WARNTHRESH* set in preferences, display a warning (unless turned off in preferences).

3. For each sample, update the in-situ velocity arrays and associated endpoint index pointers to account for deleted characteristics. Note that the pointers now refer to the in-situ endpoints *U*MIN* and *U*MAX* of each profile.

4. If the largest upper velocity endpoints of $u^*(t)$ are not the same for at least two profiles, truncate the higher one and interpolate its new endpoint to that of the second-highest, ensuring that the maximum velocity encompasses at least two profiles for analysis.

5. If needed, apply the correction for unequal baseplates, updating $t(u^*)$ for each profile.

6. Set up a single uniform velocity grid array u_g going from min(*U*MIN*) to max(*U*MAX*).

7. For each profile, set up index pointers to elements of u_g corresponding to that profile's *U*MIN* and *U*MAX*, and use a special interpolation routine to find the time array t_g corresponding to the points in u_g on this interval; this inversion of the curves is needed for the Lagrangian analysis step.

    a. The special interpolation routine uses binning and local fitting to determine an appropriate value of t_g for each value of u_g given a noisy $u^*(t)$ curve.

8. Compute wave speed $c_L(u_g)$, including in the $X(t_g)$ fit at each value of u_g only those profiles for which $U^*MIN \leq u_g \leq U^*MAX$.

9. If the first point of $u_g > 0$, then insert a point at the beginning of $c_L(u_g)$ for $u_g = 0$, setting c_L = *C0* if available, otherwise copying c_L from the first point.

10. Filter the wave speed if needed using the values of *FILTDEG* and *FILTWIN* for the current iteration.

11. Compute the EOS curves $\rho(u_g)$ and $\sigma_x(u_g)$ by integrating Equations (2), using the filtered wave speed, and set $F(u_g) = u^* = u_g$.

12. If the maximum value of $\sigma_x(u_g) < \max(\sigma_R)$, then extrapolate the EOS curves to encompass σ_R.

    a. *NSEXT* points in the extrapolated region are distributed uniformly from $\max(\sigma_x)$ to $\max(\sigma_R)$ with spacing equal to the average spacing between points of σ_x.

    b. Density in the extrapolated region is determined by a quadratic fit to approximately the last *NSEXT* + 2 points of $\sigma_x(\rho)$, ensuring at least three points for the fit.

c. Extrapolated values of c_L and u^* (and hence F) are found by Equations (2); c_L requires computation of a numerical derivative, but the extrapolated function is smooth.

Once this sequence has been completed, CHARICE is ready to begin the next iteration at step 1. To compute iteration #0, the sequence starts at step 6 using the first guess for in-situ velocity profiles from Section 4.1; note that the correction for unequal baseplates is not applied during iteration #0. If performing an in-situ calculation with baseplate correction, all iterations (subsequent to iteration #0) begin at step 5.

This page intentionally left blank.

5. Examples

The following four examples demonstrate many of the capabilities of CHARICE. Most of the examples use simulated data, which allows comparison of the results to the actual response exhibited by the material in the simulation. All data and setup files needed to run the examples are distributed with the CHARICE code. In addition, the setup file for each example is reproduced in Appendix C.

5.1. Elastic-Plastic Behavior

Strictly speaking, an elastic-plastic transition in the material response generates entropy, violating the conditions required for iterative Lagrangian analysis. In addition, the reflection of a well-defined precursor due to such a transition from a free surface or lower-impedance window can create a local region in *X*-*t* space near the window where stress in the material decreases with time. This local unloading would follow an elastic stress-strain path even if plastic deformation has already occurred, but in iterative Lagrangian analysis, the material response must be single-valued, *i.e.*, reversible. It turns out these effects are often small enough that CHARICE still produces very accurate results.

For this example, free-surface velocities due to ramp-wave loading of two aluminum samples, 1.5 and 2.5 mm thick, were simulated using the WONDY code.[17] The stress loading history was based on the current pulse of the Veloce Small Pulser[18] with a peak of 7 GPa. The bulk response of aluminum was modeled by the Mie-Grüneisen EOS referenced to a linear shock-speed/particle-velocity Hugoniot (U_s = 5288 m/s + 1.3756 U_p), with constant $\rho\Gamma = \rho_0 \Gamma_0$ (where ρ_0 = 2703 kg/m^3 and Γ_0 = 2.14). The elastic-plastic option of WONDY was used with Y_0 = 0.35 GPa and Poisson's ratio ν = 0.34.

The input free-surface velocity profiles shown in Figure 7(a) were processed initially by setting *UMIN* = 0.0005 m/s (the noise-free simulation data allows *UMIN* arbitrarily close to zero velocity), *UMAX* = 760 m/s, and *NCH* = 1024. CHARICE output after iteration #8 (relative deviation from iteration #7 was 3×10^{-4}) with no filtering is shown by the green curve in Figure 7(b), which lies right on top of the blue curve extracted from a WONDY simulation, but stops at 5.3 GPa. The iterative Lagrangian analysis only gives the material response to 5.3 GPa due to arrival of the first negative characteristic at the left boundary of the thinner sample. Setting the threshold for the "first disturbance" at 0.0005 m/s starts the first positive and hence reflected negative characteristics much earlier in time than is necessary to resolve the material response. The result of a second CHARICE run with *UMIN* = 0.8 m/s is shown by the thick red curve in Figure 7(b), which goes to 6.1 GPa.

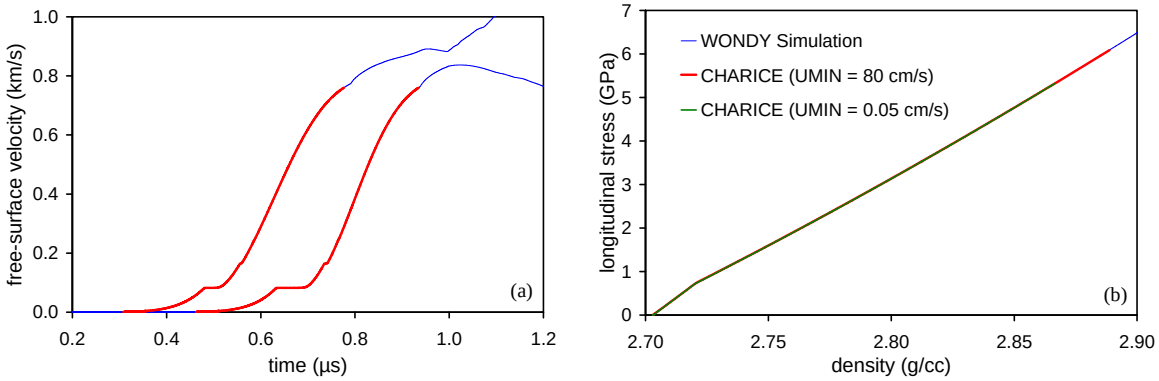

Figure 7. Example from Section 5.1; (a) input free-surface velocity profiles (processed profiles shown as thick curves), (b) output stress-density paths for two different values of *UMIN* compared to that extracted from a WONDY simulation. The value of *UMIN* affects the arrival time at $X = X_L$ of the first negative characteristic, which stops the calculation and limits the maximum stress of the result.

Despite neglecting entropy generation due to plastic work and local unloading due to a reflected precursor, CHARICE reproduced the stress-density path of the simulation very well. The differences are not discernable in Figure 7(b); the error is at most 1% in the elastic region, dropping to less than 0.05% at the upper end. Just above yield, the error is 0.15% (*UMIN* = 0.0005 m/s) to 0.5% (*UMIN* = 0.8 m/s).

5.2. Window of Higher Impedance than Sample Material

This example demonstrates the case of an interferometer window that has higher acoustic impedance than the sample material, requiring extrapolation of the sample material response to obtain a result. The simulated problem is similar to the example in Section 5.1 except for the presence of sapphire windows and the use of a different yield model for aluminum. Sapphire was modeled by the Mie-Grüneisen EOS referenced to the elastic Hugoniot (U_s = 11.19 km/s + U_p), with constant $\rho\Gamma = \rho_0\Gamma_0$ (where ρ_0 = 3985 kg/m^3 and Γ_0 = 1.5). The ramp-loading response of sapphire for input to CHARICE was found by numerically integrating this EOS along the principal isentrope to a maximum stress of 12 GPa. The aluminum yield model was the distributed-yield model of Vogler *et al*,[19] implemented as part of STAT8 in the WONDY code.

The input velocity profiles shown in Figure 8(a) were processed by setting *UMIN* = 0.0002 m/s, *UMAX* = 225 m/s, and *NCH* = 1024. CHARICE output after iteration #8 (relative deviation from iteration #7 was 2.2×10^{-4}) with no filtering is shown by the red curve in Figure 8(b). This lies right on top of the thick blue curve extracted from a WONDY simulation, but stops at 6.5 GPa, the maximum in-situ stress determined by Lagrangian analysis of in-situ velocity profiles. The backward calculation to map measured to in-situ velocity profiles, however, required CHARICE to extrapolate the sample's response curve to 10 GPa, the maximum stress at the sapphire window interface. This extrapolation is shown by the thin green curve in Figure 8(b).

The extrapolated part of the material response must influence the result deduced for material response in the non-extrapolated region, but the error thus caused in this particular case appears to be small. This may be partly due to self-consistency enforced by the iterative process, and partly due to the choice of an extrapolating function (stress quadratic in density) that produces reasonable behavior in the extrapolated region. The difference between the CHARICE result and the stress-density path from the simulation in Figure 8(b) is at most 1% in the elastic region, dropping to 0.1% just beyond yield and then further to 0.05% around 2.8 g/cc before increasing again to 0.15% at 6.5 GPa.

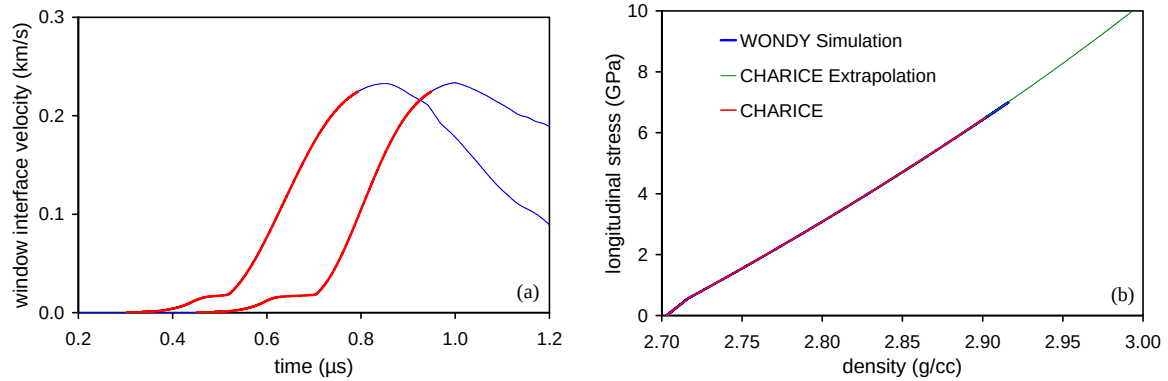

Figure 8. Example from Section 5.2; (a) input sapphire window-interface velocity profiles with processed profiles shown as thick red curves, (b) output stress-density paths, with and without the extrapolated region, compared to the stress-density path extracted from a WONDY simulation. Due to the higher impedance of sapphire relative to aluminum, extrapolation to 10 GPa was required to obtain the in-situ result to 6.5 GPa.

5.3. Correction for Unequal Baseplate Thickness

For this example, the ALEGRA code[20] was used to perform full magneto-hydrodynamic simulations of 1.0-mm and 1.2-mm thick tungsten samples mounted on aluminum baseplates of nominally 0.6 mm thickness, but with the baseplate behind the 1.0-mm sample actually 0.02 mm thicker than the baseplate behind the 1.2-mm sample. A time-varying magnetic field, corresponding to the electrical load current pulse and load geometry of Z shot 1504, was applied to the drive-side boundary of each baseplate. Both aluminum and tungsten were modeled by tabular equations of state (Sesame 3700 for aluminum[21] and Sesame 3550 for tungsten[22]) along with the Steinberg-Guinan-Lund yield model[23] (including rate dependence for tungsten) and the Lee-More-Desjarlais conductivity model[24] tuned to quantum molecular-dynamic computational data.[25]

The simulated free-surface velocity histories of the two tungsten samples are shown in Figure 9(a). These were input to CHARICE and processed by setting *UMIN* = 0.002 m/s, *UMAX* = 1050 m/s, and *NCH* = 1024. The maximum velocity was set significantly below the peak velocity because the region near the peak of each profile has been contaminated by overtaking elastic release disturbances, violating the requirement of simple-wave flow outside the interface interaction region. CHARICE output after iteration #3 (relative deviation from iteration #2 was 4.1×10^{-4}) with no filtering, and the correction turned on for unequal baseplates (*DXB* = 0.02 mm for profile #1), is shown by the red curve in Figure 9(b). This lies very close to the blue curve extracted from an ALEGRA simulation for a thicker sample. Without the correction for unequal baseplates, CHARICE produces the result shown by the green curve, which is in error by 15% at its upper end. Clearly, differences in baseplate thickness of only a few percent from sample to sample can seriously compromise the deduced material response path if not accounted for.

The CHARICE result (with baseplate correction) reproduces the stress-density path of tungsten in the simulation to better than 1% everywhere except the elastic region, where the difference reaches 3%. This level of agreement is very satisfactory considering that the tungsten yield-strength model depends on pressure, temperature, and strain rate. At a longitudinal stress of 65 GPa, the temperature in the simulation is 134 K higher than the temperature on the tungsten's principal isentrope at the corresponding mean stress (pressure). This is a relatively small deviation from isentropic conditions, especially in terms of its effect on the mechanical (stress-density) response. Despite the assumption of isentropic flow required for iterative Lagrangian analysis, CHARICE can determine quasi-isentropic compression loading paths in materials with high strength to reasonably high accuracy.

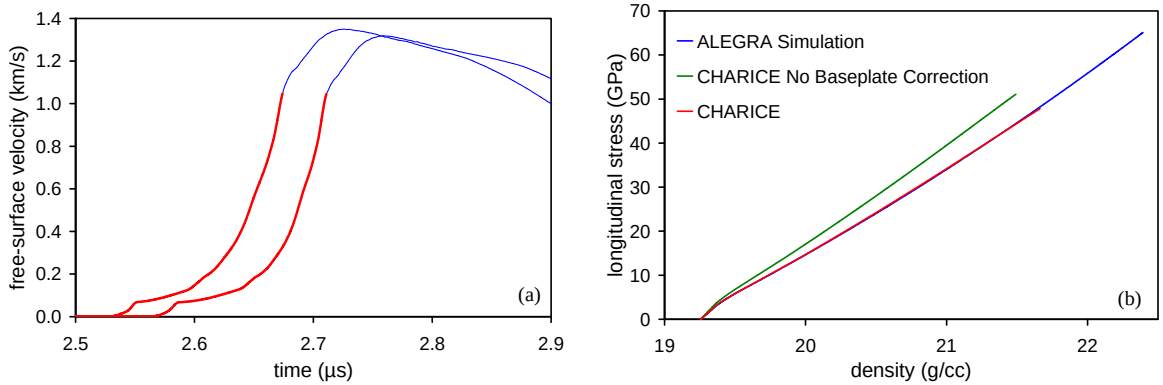

Figure 9. Example from Section 5.3; (a) input free-surface velocity profiles with processed profiles shown as thick red curves, (b) output stress-density paths, with and without the correction for unequal baseplate thickness, compared to the stress-density path extracted from an ALEGRA simulation. A 3% difference in baseplate thickness between the two samples causes a 15% error in deduced stress if not accounted for.

5.4. Multiple Velocity Fit Ranges

The fourth and final example revisits high-pressure experimental data on 6061-T6 aluminum from Z shot 1190, previously analyzed by this author using the minimization approach with backward finite-difference integration.[26] The experiment used four samples consisting of the anode electrode itself, machined to four different thicknesses. The experimental free-surface velocity profiles input to CHARICE are shown in Figure 5 along with all the parameter settings on the Setup GUI used to process the profiles and run the calculation; units are cgs. The *TSCALE* and *USCALE* parameters convert data loaded from the input files from (μs, km/s) to (s, cm/s). The *TSHIFT* parameter array is set to shift profiles #1 and #3 by -0.8 ns, as determined in Reference 26 by a self-consistency argument.

Unlike the previous examples, *UMIN* and *UMAX* are set to different values for each profile, so that only certain profiles are included in the $X(t)$ fit to compute wave speed in particular ranges of velocity. *UMIN* is chosen to be as close to zero as possible considering noise in the experimental data, except for profile #4, for which *UMIN* is chosen above the small shock and the disturbance due to its first reflection off the oncoming wave. *UMAX* is chosen for each profile to avoid regions contaminated by reverberation between the free surface and the joule-heated region that is advancing into the aluminum from the drive surface,[27] which begins earlier in time for the thinner samples. Note that CHARICE cannot automatically determine the time at which this reverberation compromises data. At least two profiles are included at the smallest *UMIN* = 6 m/s and at the largest *UMAX* = 12.2 km/s. The *TMIN* parameter array is used to restrict the time range of each profile over which CHARICE searches for the first data point equal to or greater than *UMIN*. All four input profiles are filtered by setting *SGDEG* = 3 and *SGWIN* = 2 ns, and are interpolated onto uniform time grids with *NCH* = 768 points between min(*UMIN*) and max(*UMAX*). Finally, the uncertainty computations are turned on and experimental uncertainties from Reference 26 are provided for each profile in the parameter arrays *DXS*, *DTS*, *VPF*, *DVPF*, and *DFC*.

The CHARICE Calculation GUI for this problem is shown in Figure 6 after iteration #11 and computation of uncertainty bounds. After every iteration (including iteration #0), the $c_L(u^*)$ curve was filtered using *FILTDEG* = 3 and *FILTWIN* = 800 m/s to reduce high-frequency noise. Comparison to the first-guess iteration #0 (cyan curves) emphasizes the importance of correcting for the bending of characteristics in the interaction region near each free surface, especially for megabar-level experiments. The material response in terms of $c_L(u^*)$ is not entirely converged after iteration #11 due to an apparent instability in the upper velocity range where only profiles #3 and #4 are used; the blue and

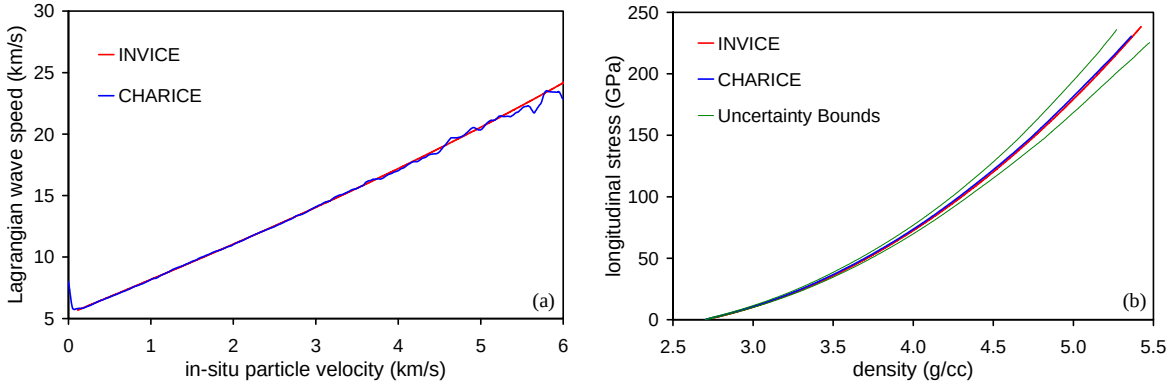

Figure 10. Example from Section 5.4; (a) CHARICE result for $c_L(u^*)$ compared to the previous result from Reference 26 using the INVICE code, (b) the same comparison in the $\sigma_x(\rho)$ plane, along with uncertainty bounds determined by CHARICE using the second method from Section 2.3.

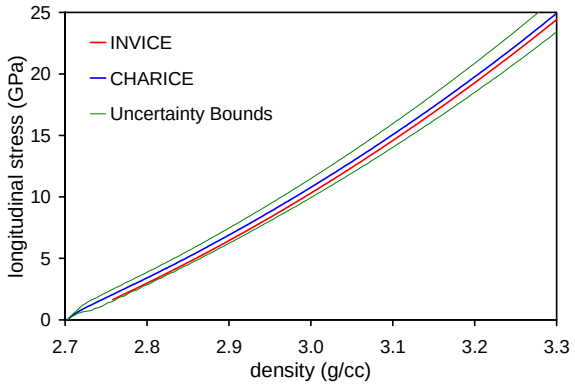

Figure 11. Zoomed view of lower left corner in Figure 10(a), showing offset between CHARICE and INVICE results due to neglect of the elastic precursor in the INVICE analysis.

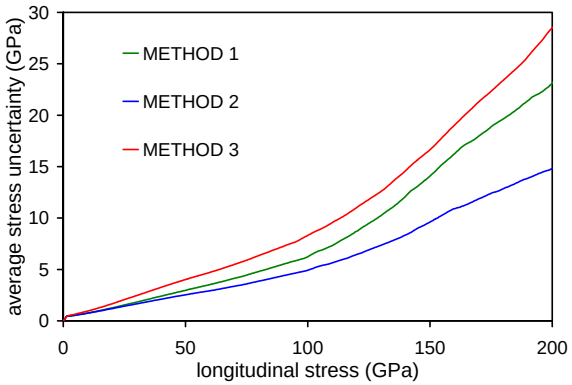

Figure 12. Uncertainty in longitudinal stress (average deviation of lower and upper bounds from nominal result) for the example in Section 5.4, computed using the three methods of Section 2.3.

red curves for previous and current iteration tend to flip-flop with each iteration. The difference, however, is very small in the $\sigma_x(\rho)$ plane. The uncertainty bounds shown by the magenta curves in Figure 6 were computed by the Method 2, wherein time uncertainties are taken from the spread of backward-projected in-situ profiles instead of the experimental uncertainties *DTS* (see Section 2.3).

In Figures 10-11, the CHARICE result is compared to the previous result from Reference 26, which was deduced from an analysis using the INVICE code.[8] The $c_L(u^*)$ curve in Figure 10(a) appears smooth for the INVICE result because it is represented by a polynomial function as part of the minimization process; the CHARICE result follows more closely local variations in the experimental data. The other major difference between the approaches is that the elastic precursor region of the measured velocity profiles was ignored in the INVICE analysis; the fit for $c_L(u^*)$ begins at $u^* = 110$ m/s, and is extrapolated to zero velocity in order to obtain $\sigma_x(\rho)$. This results in a stress offset between the INVICE and CHARICE results, approximately equal to the difference between the longitudinal stress and mean stress at yield, and apparent in the zoomed view of Figure 11.

Because this example is based on real experimental data, it provides an excellent case to illustrate differences between the three methods available in CHARICE for computing uncertainties. The uncertainty bounds in Figure 10(b) were computed using Method 2, consisting of Equations (12), (14), (15), and (17) with time uncertainties based on spread in backward-computed in-situ velocity profiles. In Figure 12, these uncertainty bounds are compared with those computed by the other two methods described in Section 2.3; Method 1 uses a single-valued experimental time uncertainty for each profile but is otherwise the same as Method 2, and Method 3 computes linear sensitivities of the result to experimental uncertainties in time, velocity, and sample thickness. Method 2 results in the smallest uncertainty bounds, suggesting that the experimental time uncertainties have a significant systematic component (random errors are all that should affect the spread of backward-projected profiles). Method 3 results in larger uncertainty bounds than Method 1, though both use the experimental time uncertainties. For a given set of uncertainties in time, velocity, and sample thickness, Method 3 should be more accurate as long as the uncertainties are uncorrelated and truly random. The latter assumption requires further investigation. For this particular example, the result using Method 2 was deemed most realistic due to systematic timing errors.

6. Limitations of the Approach

Formally, the iterative Lagrangian analysis method implemented in CHARICE requires that all the samples be subjected to identical loading histories during the time of interest, that the sample material's mechanical response be single-valued (reversible and without time dependence), and that the compression wave propagates as a simple wave in the bulk material outside the interface interaction region. In addition, if interferometer windows are present, simple-wave behavior is required in the window material near the interface. Despite these restrictions, the example problems in Sections 5.1 through 5.3 show that very accurate results can still be obtained for compression response when deviations from reversible, isentropic behavior are relatively small, such as those due to material strength. The example in Section 5.3 shows that non-identical loading histories can be corrected for if they are due to non-uniform thickness of baseplates.

CHARICE has the capability to extrapolate the loading response of the material in order to complete a mapping of measured to in-situ velocity profiles when the interface stress is higher than the in-situ stress, and the example problem in Section 5.2 shows that the approach can work quite well. It must be emphasized, however, that the result thus obtained for the sample's loading response near the maximum in-situ stress must depend on the extrapolation. This dependence may be weak in some cases; nevertheless, extreme caution is urged when using the extrapolation option.

Velocity data from ramp loading of material exhibiting larger deviations from isentropic behavior, such as the volume collapse at a structural phase transition, are in general not amenable to analysis by the iterative Lagrangian analysis method. Many such data exhibit a growing shock immediately following transition to the second phase. When applied to data lacking a shock due to non-equilibrium effects such as transition kinetics, the method fails to converge on a material response curve for $c_L(u^*)$ at velocities above the phase transition. Analysis of phase transitions under ramp-wave loading will likely require an iterative forward calculation technique, where the parameters for a material model are optimized to match experimental velocity profiles in forward 1-D simulations.

With in-situ velocity measurements, it is possible to use Lagrangian analysis techniques to determine a material's elastic-plastic response to unloading from a known peak state. This may even work in an approximate sense for ramp-loading experiments where the peak state attenuates with propagation distance due to the overtaking elastic release. Window interface measurements of unloading in a sample material of significantly different acoustic impedance than the window material, however, cannot be analyzed to any reasonable accuracy using iterative Lagrangian analysis. The problem is that each material point in the interaction region, where characteristics intersections need to be computed, unloads from a different peak state somewhere between the in-situ and interface peak states, but the Lagrangian analysis step can be applied only to the in-situ peak state. The unloading behavior thus cannot be described by a single-valued function of u^*. As for phase transitions, these types of experiments will probably require an iterative forward calculation approach.

7. Suggestions for Future Extensions

CHARICE was developed with magnetically driven ramp wave experiments in mind, but there are other experimental techniques for generating ramp loading of samples. One of these is the graded-density impactor,[28] which typically produces a wave profile consisting of a shock followed by ramp. CHARICE could be extended to analyze this case as long as there exists a constant-state dwell time between the shock and the onset of ramp compression. Figure 13 shows a schematic of characteristics and shocks in the *X-t* plane for an initial shock with an elastic precursor. In order to map interface-velocity measurements to in-situ profiles at X_R, trajectories of the positive characteristics in the 'undisturbed' post-shock region must be computed backward through one or two rarefaction waves. This may be possible using modest modifications to the routine that computes the ramp-wave interaction region, but would require knowledge of the incident and reflected shock states on both sides of the measurement interface for the elastic and plastic pre-shocks. If windows were used, then the transmitted shock states as well as the ramp-loading response of the window material for the (non-ambient) initial condition of the ramp would be needed.

In CHARICE, the first guess for the sample material response is determined from the data themselves by using a simple first guess at the mapping of measured to in-situ velocity profiles. This is generally considered the preferable approach since the result depends only on the data, but some users may wish to perform an analysis using a different first guess for the sample material response, say, based on some model. CHARICE could be extended to allow input of such a first guess.

Other ideas for extending CHARICE center on increasing the number of output options. These could include scale factors to convert output data to desired units, output of results from different iterations without having to rerun the calculation, output of material state and velocity at all the characteristics intersections, and even graphical output of the plots presently displayed in the Setup GUI or Calculation GUI, or an *X-t* diagram. Finally, another useful and convenient interface feature not currently available (and non-trivial to implement) would be a capability to abort long calculations in real time.

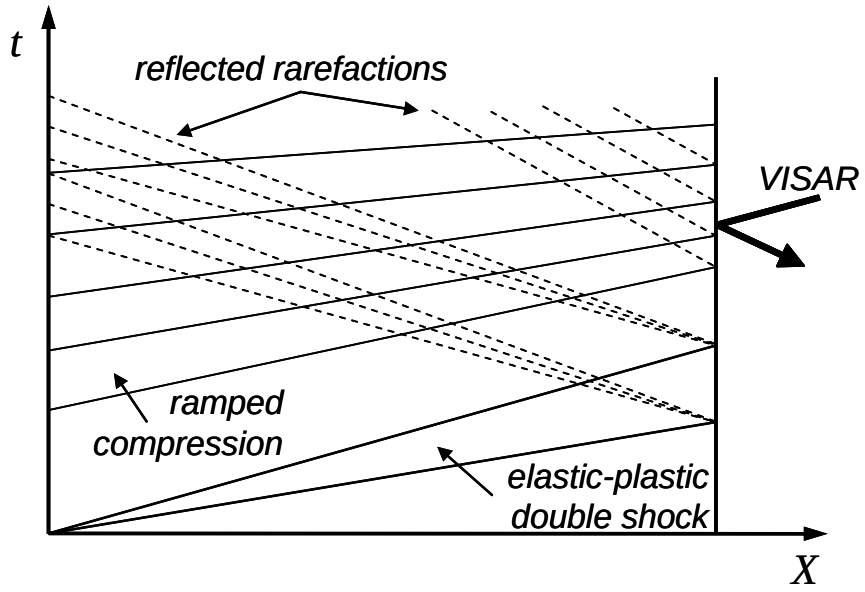

Figure 13. Schematic of *X-t* diagram for an elastic-plastic double shock followed by a ramp; solid lines show the in-situ case, while dashed lines indicate reflected (negative) release characteristics for a window of lower acoustic impedance than the sample material. Bending of characteristics is not shown.

References

[1] S. D. Rothman *et al*, Measurement of the principal isentropes of lead and lead-antimony alloy to ~400 kbar by quasi-isentropic compression, in *Journal of Physics D: Applied Physics*, Vol. 38, pp. 733-740, 2005.

[2] S. D. Rothman, *Characteristics Analysis of Isentropic Compression Experiments (ICE). PPN 05/05*, Atomic Weapons Establishment (AWE) Report 151/05, February 2005.

[3] S. D. Rothman and J. Maw, Characteristics analysis of isentropic compression experiments (ICE), in *Journal of Physics IV (Proceedings)*, Vol. 134, pp. 745–750, 2006.

[4] D. B. Hayes and C. A. Hall, Correcting free surface effects by integrating the equations of motion backward in space, in *Shock Compression of Condensed Matter—2001*, edited by M. D. Furnish, N. N. Thadhani, and Y. Horie, American Institute of Physics, Melville, NY, pp. 1177-1180, 2002.

[5] D. B. Hayes, *Backward Integration of the Equations of Motion to Correct for Free Surface Perturbations*, Sandia National Laboratories Report SAND2001-1440, May 2001.

[6] D. B. Hayes, J. E. Vorthman, and J. N. Fritz, *Backward Integration of a VISAR Record: Free-Surface to the Spall Plane*, Los Alamos National Laboratory Report LA-13830-MS, May 2001.

[7] D. B. Hayes, C. A. Hall, J. R. Asay, and M. D. Knudson, Continuous index of refraction measurements to 20 GPa in Z-cut sapphire, in *Journal of Applied Physics*, Vol. 94, No. 4, pp. 2331–2336, 2003.

[8] J.-P. Davis, *User Manual for INVICE 0.1-beta: A Computer Code for Inverse Analysis of Isentropic Compression Experiments*, Sandia National Laboratories Report SAND2005-2068, April 2005.

[9] R. Fowles and R. F. Williams, Plane stress wave propagation in solids, in *Journal of Applied Physics*, Vol. 41, No. 1, pp. 360-363, 1970.

[10] M. Cowperthwaite and R. F. Williams, Determination of constitutive relationships with multiple gauges in nondivergent waves, in *Journal of Applied Physics*, Vol. 42, No. 1, pp. 456-462, 1971.

[11] L. Seaman, Lagrangian analysis for multiple stress or velocity gages in attenuating waves, in *Journal of Applied Physics*, Vol. 45, No. 10, pp. 4303-4313, 1974.

[12] J. Cagnoux, P. Chartagnac, P. Hereil, and M. Perez, Lagrangian Analysis: Modern tool of the dynamics of solids, in *Annales de Physique*, Vol. 12, pp. 451-524, 1987.

[13] J. B. Aidun and Y. M. Gupta, Analysis of Lagrangian gauge measurements of simple and nonsimple plane waves, in *Journal of Applied Physics*, Vol. 69, No. 10, pp. 6998-7014, 1991.

[14] Y. B. Zel'dovich and Y. P. Raizer, *Physics of Shock Waves and High-Temperature Hydrodynamic Phenomena*, Academic Press, New York, 1967 (republished by Dover Publications in 2002).

[15] P. R. Bevington and D. Keith Robinson, *Data Reduction and Error Analysis for the Physical Sciences (Third Edition)*, McGraw-Hill, New York, 2003.

[16] W. H. Press, S. A. Teukolsky, W. T. Vetterling, and B. P. Flannery, *Numerical Recipes in Fortran 77: The Art of Scientific Computing*, 2nd ed., Cambridge University Press, New York, 1992.

[17] M. E. Kipp and R. J. Lawrence, *WONDY V — A One-Dimensional Finite-Difference Wave Propagation Code*, Sandia National Laboratories Report SAND81-0930, June 1981.

[18] T. Ao *et al.*, submitted to *Review of Scientific Instruments.*

[19] T. J. Vogler and J. R. Asay, A distributional model for elastic-plastic behavior of shock-loaded materials, in *Shock Compression of Condensed Matter—2003*, edited by M. D. Furnish, Y. M. Gupta, and J. W. Forbes, American Institute of Physics, Melville, NY, pp. 617-620, 2004.

[20] T. A. Haill *et al.*, *Alegra-MHD: Version 4.6*, Sandia National Laboratories Report SAND2004-5997, December 2004.

[21] G. I. Kerley, Theoretical equation of state for aluminum, in *International Journal of Impact Engineering*, Vol. 5, pp. 441-449, 1987.

[22] G. I. Kerley, *Equations of State for Be, Ni, W, and Au*, Sandia National Laboratories Report SAND2003-3784, October 2003.

[23] P. A. Taylor, *CTH Reference Manual: The Steinberg-Guinan-Lund Viscoplastic Model*, Sandia National Laboratories Report SAND92-0716, 1992.

[24] M. P. Desjarlais, Practical improvements to the Lee-More conductivity near the metal-insulator transition, in *Contributions to Plasma Physics*, Vol. 41, pp. 267-270, 2001.

[25] M. P. Desjarlais, J. D. Kress, and L. A. Collins, Electrical conductivity for warm, dense aluminum plasmas and liquids, in *Physical Review E*, Vol. 66, p. 025401(R), 2002.

[26] J.-P. Davis, Experimental measurement of the principal isentrope for aluminum 6061-T6 to 240 GPa, in *Journal of Applied Physics*, Vol. 99, p. 103512, 2006.

[27] J.-P. Davis *et al*, Magnetically driven isentropic compression to multimegabar pressures using shaped current pulses on the Z accelerator, in *Physics of Plasmas*, Vol. 12, p. 056310, 2005.

[28] L. M. Barker, High-pressure quasi-isentropic impact experiments, in *Shock Waves in Condensed Matter—1983*, edited by J. R. Asay, R. A. Graham, and G. K. Straub, Elsevier Science Publishers, pp. 217-224, 1984.

Appendix A: Preferences

Pressing the PREFERENCES button on the Setup GUI brings up the window shown in Figure A-1, allowing the user to set certain global preferences for CHARICE. Most of these are self-explanatory.

The General Settings section consists mainly of switches to turn on or off various warning or confirmation dialog boxes. If the box is checked to display a warning when characteristics are deleted, the warning is only shown if the number of deleted characteristics exceeds the threshold value given. The first preference under General Settings is the full path of the directory to use as the default starting directory the first time a file-pick dialog box opens for selecting files to load or save, or for selecting a directory. Pressing the open-file icon brings up a separate dialog box to select this directory. If the specified directory does not exist in the file system, file-pick dialogs will default to the directory in which CHARICE resides. Subsequent to the first use of a file-pick dialog during a session, the default starting directory will be the last one used in any file-pick dialog.

The Defaults section consists of default values for the setup form, which are used when CHARICE first launches, when clearing the setup form, and as defaults for missing parameters when loading a form. The preference for maximum number of profiles limits the available number of profiles in the *NPROF* drop-down list of the Setup GUI, and is used to set *NPROF* when CHARICE first launches. The default filename endings are used when pressing RETURN in the *FROOT* field of the Setup GUI, and to set default filenames that are missing when loading a form.

The Graphics Settings section allows the user to change how IDL handles backing store and object-graphics rendering. Backing store of window graphics is handled by the operating system if set to "System" and by IDL if set to "Bitmap." The object rendering method may affect zooming of plots. These settings need only be changed if the user experiences problems with the default values.

The Variable Types section allows the user to change the numerical precision of floating-point numbers used for computations in CHARICE. The bit-length of integer variables can also be changed, though the only reason to do this would be to allow more than 32,768 elements in arrays. Changes to these variable types do not take effect until exiting and re-launching CHARICE.

Click the OK button to accept changes to the preferences, or CANCEL to close the window without changing preferences. The preference values are saved to an external file when exiting CHARICE so they are available the next time CHARICE is launched.

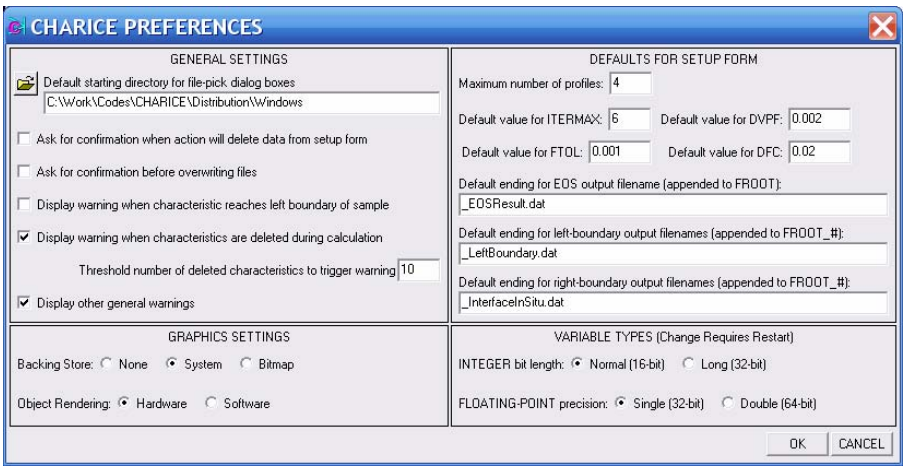

Figure A-1. GUI window for setting CHARICE preferences, shown for Windows XP.

Appendix B: Specification of Setup File Format

A setup file is a text file, with each parameter name on a line by itself (trailing comments are allowed on this line) followed immediately by the parameter's corresponding value on the following line. Individual elements of numerical array-valued parameters must be placed on a single line with space, tab, or comma delimiting. The values for filename array parameters, however, must be placed one element per line. Parameters may appear in any order, except that **`nprof`** must appear before any of the array-valued parameters having **`nprof`** elements. Binary flag parameters require only the parameter name on a single line (with no additional lines). Blank lines or lines starting with !, *, %, or ; are ignored. File names can use absolute or relative paths. Note that use of a path separator character in a file name necessarily makes the input file non-portable between computing platforms. A setup file created by CHARICE uses path separators, and therefore must be modified manually to work on a different platform than the one on which the file was created.

The following list, similar to the ones in Sections 3.1–3.4, provides a short description of each possible parameter and notes which ones are required or optional. Array-valued parameters requiring **`N`** elements are indicated by the subscript range notation **`[1:N]`**. Some of these allow a single value that is then automatically copied to all the array elements. When parsing a parameter name that is *nchar* characters long, CHARICE looks only at the first *nchar* characters of the line, thus subsequent text on the same line can be added for use as a comment.

`froot` = root file name for output files (defaults to root name of the setup file itself)

`nch` = number of characteristics to distribute across largest velocity compute range, based on **`umin`** and **`umax`**, in processed velocity profiles (defaults to smallest number of points across velocity compute range in original input velocity profiles)

`r0` = ambient sample density (required)

`c0` = ambient sample sound speed (required in windowed case to estimate first-guess in-situ correction factor, otherwise optional); if present, used at zero-velocity point when computing EOS from $c_L(u)$)

`itermax` = maximum number of iterations to find converged EOS (defaults to preference value)

`ftol` = tolerance in the mean root square of the fractional deviation of Lagrangian wave speed from the previous iteration to stop iterations (defaults to preference value)

`nprof` = number of velocity profiles (required, must appear before any array-valued parameter)

`ufiles[1:nprof]` = file names for input velocity profiles (required)

`tscale` = single time-scale factor applied to all input velocity profiles (defaults to 1)

`uscale` = single velocity-scale factor applied to all input velocity profiles (defaults to 1)

`xs[1:nprof]` = sample thicknesses (required)

`tshift[1:nprof]` = time shift applied to each input velocity profile (defaults to zero shift)

`tmin[1:nprof]` = lower time cutoff for each input velocity profile; earlier times are discarded prior to any other processing (defaults to first point of each velocity file)

`umin[1:nprof]` = lower velocity limit of compute range for each profile (if only **`umin[1]`** provided, then **`umin[2:nprof]`** default to **`umin[1]`**; otherwise defaults to first point of contiguous positive increasing velocity of each profile)

`umax[1:nprof]` = upper velocity limit of compute range for each profile (if only **`umax[1]`** provided, then **`umax[2:nprof]`** default to **`umax[1]`**; otherwise defaults to peak velocity of each profile)

sgdeg[1:nprof] = degree of Savitsky-Golay filter applied to each input velocity profile (if only **sgdeg[1]** provided, then **sgdeg[2:nprof]** default to **sgdeg[1]**; otherwise defaults to 0, which indicates no filtering)

sgwin[1:nprof] = time window of Savitsky-Golay filter applied to each input velocity profile (if only **sgwin[1]** provided, then **sgwin[2:nprof]** default to **sgwin[1]**; otherwise defaults to 2% of full time range, or minimum required to encompass at least **sgdeg[1:nprof]** points)

uncertainty = binary flag to request computation of uncertainties (optional, automatically turned on if any of the parameters **dxs**, **dts**, **dvpf**, or **dfc** are present)

dxs[1:nprof] = absolute sample thickness uncertainty for each velocity profile (if only **dxs[1]** provided, then **dxs[2:nprof]** default to **dxs[1]**; otherwise default to 0)

dts[1:nprof] = absolute time uncertainty for each velocity profile (if only **dts[1]** provided, then **dts[2:nprof]** default to **dts[1]**; otherwise default to 0)

vpf[1:nprof] = VPF for each velocity profile (required if uncertainties to be computed; if only **vpf[1]** provided, then **vpf[2:nprof]** default to **vpf[1]**)

dvpf[1:nprof] = fractional uncertainty in VPF for each velocity profile (if only **dvpf[1]** provided, then **dvpf[2:nprof]** default to **dvpf[1]**; otherwise defaults to preference value)

dfc[1:nprof] = absolute uncertainty in fringe count for each velocity profile (if only **dfc[1]** provided, then **dfc[2:nprof]** default to **dfc[1]**; otherwise defaults to preference value)

baseplate = binary flag to request computation of correction for unequal baseplate thicknesses (optional; automatically turned on if the parameter **dxb** is present)

dxb[1:nprof] = deviation from nominal of baseplate thickness for each velocity profile (if fewer than **nprof** elements provided, remaining elements default to 0)

beosfile = file name for baseplate EOS (required if **dxb** or **baseplate** present)

beoscol[1:4] = column indices for the variables ρ, σ_x, u^*, and c_L in **beosfile** (required if **dxb** or **baseplate** present; set an element to -1 to indicate corresponding variable is not available)

beosfac[1:4] = scale factors applied to the variables ρ, σ_x, u^*, and c_L in **beosfile** (used only if **dxb** or **baseplate** present; defaults to 1)

beoseul = binary flag to indicate c_L column in **beosfile** gives Eulerian instead of Lagrangian wave speed (used only if **dxb** or **baseplate** present; turned off by default)

beosvol = binary flag to indicate ρ column in **beosfile** gives specific volume instead of density (used only if **dxb** or **baseplate** present; turned off by default)

freesurface = binary flag to indicate velocity measurements were taken at a free surface (optional; automatically turned on if none of the parameters **insitu**, **window**, or **weosfile** are present)

insitu = binary flag to indicate velocity measurements are in-situ (overrides value of the **freesurface** parameter)

window = binary flag to indicate velocity measurements were taken at a window interface (optional; automatcially turned on if the parameter **weosfile** is present; overrides the values of **freesurface** and **insitu**)

weosfile = file name for window EOS (required if **window** present)

weoscol[1:4] = column indices for the variables ρ, σ_x, u^*, and c_L in **weosfile** (required if **weosfile** present; set an element to -1 to indicate corresponding variable is not available)

weosfac[1:4] = scale factors applied to the variables ρ, σ_x, u^*, and c_L in **weosfile** (used only if **weosfile** present; defaults to 1)

weoseul = binary flag to indicate c_L column in **weosfile** gives Eulerian instead of Lagrangian wave speed (used only if **weosfile** present; turned off by default)

weosvol = binary flag to indicate ρ column in **weosfile** gives specific volume instead of density (used only if **weosfile** present; turned off by default)

outeos = binary flag to request file output of the EOS result (optional, automatically turned on if the parameter **outeosfile** is present)

outeosfile = file name for output of EOS results (optional; if **outeos** present, defaults to **froot** + filename ending from preferences)

outright = binary flag to request file output of in-situ time histories at each sample's right boundary (optional, automatically turned on if the parameter **outrightfiles** is present)

outrightfiles[1:nprof] = file names for output of in-situ time-history at each sample's right boundary (optional; if **outright** present, defaults to **froot** + filename ending from preferences)

outrightcol[1:4] = column indices for the variables ρ, σ_x, u^*, and c_L in **outrightfiles**, but relative to 2nd column since time is always in 1st column (used only if **outright** or **outrightfiles** present; defaults to [-1, 1, -1, -1], indicating output of longitudinal stress only)

outleft = binary flag to request file output of in-situ time histories at each sample's left boundary (optional, automatically turned on if the parameter **outleftfiles** is present)

outleftfiles[1:nprof] = file names for output of in-situ time-history at each sample's left boundary (optional; if **outleft** present, defaults to **froot** + filename ending from preferences)

outleftcol[1:4] = column indices for the variables ρ, σ_x, u^*, and c_L in **outleftfiles**, but relative to 2nd column since time is always in 1st column (used only if **outleft** or **outleftfiles** present; defaults to [-1, 1, -1, -1], indicating output of longitudinal stress only)

Appendix C: Example Setup Files

The setup files used to run the examples in Sections 5.1–5.4 are reproduced below. These setup files, along with all the necessary data files for interface velocity and window or baseplate EOS, reside in the Examples subdirectory distributed with CHARICE.

```
*** EXAMPLE 5.1 ***
*** Al-FS-STAT1_Input.dat

froot
Al-FS-STAT1-umin80

nch
1024

r0
2.703000

c0
642790.000000

itermax
8

ftol
0.0001

nprof
2

ufiles (cgs units)
u_1500um-STAT1.dat
u_2500um-STAT1.dat

xs
0.15, 0.25

umin
80.0

umax
76000

outeosfile
Al-FS-STAT1-umin05_EOSResult.dat

outleft

outleftfiles
Al-FS-STAT1-umin80_1_LeftBoundary.dat
Al-FS-STAT1-umin80_2_LeftBoundary.dat

outleftcol
-1, 1, -1, -1

outright

outrightfiles
Al-FS-STAT1-umin80_1_InterfaceInSitu.dat
Al-FS-STAT1-umin80_2_InterfaceInSitu.dat

outrightcol
-1, 1, -1, -1
```

```
*** EXAMPLE 5.2 ***
*** Al-Sap_Input.dat

froot
Al-Sap

nch
1024

r0
2.703000

c0
646430.000000

itermax
8

ftol
0.0002

nprof
2

ufiles (cgs units)
u_1500um-STAT8.dat
u_2500um-STAT8.dat

xs
0.15, 0.25

tmin
8.5851E-011, 8.5851E-011

umin
20

umax
22500

window

weosfile
p-rho_Sapphire.dat

weoscol
1, 2, -1, -1

outeosfile
Al-Sap_EOSResult.dat

outleftfiles
Al-Sap_1_LeftBoundary.dat
Al-Sap_2_LeftBoundary.dat

outleftcol
-1, 1, -1, -1
```

***** EXAMPLE 5.3 *****
***** DXB-Correction_Input.dat**

```
froot
DXB-Correction

nch
1024

r0
19.254999

itermax
8

ftol
0.0005

nprof
2

ufiles (MKS units)
Al-W-1000FS-dxb+20um.dat
Al-W-1200FS.dat

uscale (convert to cgs units)
100

xs
0.1, 0.12

tmin
2.51922E-006, 2.55E-006

umin
0.2

umax
105000

dxb
0.002, 0

beosfile
Al3700SG-60GPa.dat

beoscol
1, 2, 3, -1

beosfac
0.001, 10, 100, 1

outeosfile
DXB-Correction_EOSResult.dat
```

***** EXAMPLE 5.4 *****
***** Z1190_CHARICE_Input.dat**

```
froot
Z1190_CHARICE

nch
768

r0
2.703000

itermax
11

ftol
0.0005

nprof
4

ufiles (in µs, km/s)
N1_0304CombinedSmooth_Al900um.v
N2_04Smooth_Al1200um.v
N3_0304CombinedSmooth_Al1500um.v
N4_0304CombinedSmooth_Al1800um.v

tscale (convert to seconds)
1E-006

uscale (convert to cm/s)
100000

xs
0.092, 0.1219, 0.1518, 0.1821

tshift
-8E-010, 0, -8E-010, 0

tmin
4.26E-008, 8E-008, 1.126E-007, 1.4E-007

umin
600, 600, 1500, 380000

umax
400000, 720000, 1.22E+006, 1.22E+006

sgdeg
3

sgwin
2E-009

dxs
0.0001

dts
2.8E-010, 3.2E-010, 6.6E-010, 5.4E-010

vpf
111000, 33000, 111000, 111000

dvpf
0.002

dfc
0.03

outeosfile
Z1190_CHARICE_EOSResult.dat
```

Appendix D: Installation and Execution

CHARICE is available to U.S. government agencies and their contractors. For information on the status of availability to other users, please contact the author by e-mail at **jpdavis@sandia.gov**.

The distribution CD-ROM for CHARICE offers two different installation approaches, depending on whether or not you wish also to install ITT Visual Information Solutions' Interactive Data Language (IDL®) on your computer. Note that a license is not required to install IDL and run applications such as CHARICE under the IDL Virtual Machine™, a free component of IDL that allows execution of compiled IDL applications. Version 6.4 of IDL (including the IDL Virtual Machine) is available by download from the World-Wide Web for the Microsoft Windows, Mac OS X, Linux, Sun Solaris, IBM AIX, and SGI IRIX computing platforms at the following URL.

http://www.ittvis.com/download/download.asp?ProductVersion=279

A third option for running CHARICE, available only for the Microsoft Windows platform, is to launch the program directly from the CD-ROM, without installing anything on your computer. The sections below give detailed installation and execution instructions.

With IDL Installed

If IDL is already installed on your computer, copy the **charice.sav** application from the root level of the CD-ROM to any desired location in your file system. To use the custom icon under Windows, also copy the file **CHARICE.ico** from the **\Windows** subdirectory on the CD-ROM to the same location in your file system as **charice.sav**. To launch CHARICE under Windows or Mac OS X, double-click on **charice.sav** or a shortcut/alias to that file. To launch CHARICE from a UNIX command line, type **idl –vm=<*path*>/charice.sav** where **<*path*>** is the relative or absolute path from the current directory to the directory in which **charice.sav** resides. Unless you have a valid runtime or development license for IDL, you will then need to click on the Virtual Machine splash window to dismiss it and start CHARICE.

Without IDL Installed

To use CHARICE without installing IDL on your computer, follow the instructions below appropriate to your computing platform.

Microsoft Windows Systems

Copy the following four files and one folder from the CD-ROM (where **<*CD-ROM*>** is the drive letter of the CD-ROM drive) to a new directory at any desired location on your hard disk.

<*CD-ROM*>:\Windows\CHARICE.exe
<*CD-ROM*>:\Windows\CHARICE.ico
<*CD-ROM*>:\Windows\CHARICE.ini
<*CD-ROM*>:\Windows\charice.sav
<*CD-ROM*>:\Windows\IDL64

To launch CHARICE, double-click **CHARICE.exe** or a shortcut to that file, and then click on the Virtual Machine splash window. You may edit a shortcut's properties to change its icon to that in the

icon file **CHARICE.ico**. To launch CHARICE directly from the CD-ROM without copying anything, double-click **CHARICE.exe** on the CD-ROM. If CHARICE does not run properly, you may be missing certain Windows system libraries. The missing libraries can be installed by running the installer **<*CD-ROM*>:\Windows\System\sytemdll32_setup.exe** on the CD-ROM.

UNIX-Based Systems (Including Mac OS X)

The files for UNIX-based systems are provided on the CD-ROM as tape-archive (.tar) files under the subdirectory **<*CD-ROM*>/UNIX/** (where **<*CD-ROM*>** is the path to the CD-ROM drive). Use the following commands from the UNIX command line to extract the necessary files to a new directory at any desired location in your file system.

tar –xf <*CD-ROM*>/UNIX/charice.tar –C <*path*>

tar –xf <*CD-ROM*>/UNIX/<*platform*>.tar –C <*path*>

Here, **<*path*>** is the relative or absolute path from the current directory to the new directory where CHARICE is to be installed, and **<*platform*>** is given by your computing platform as follows.

macosx.ppc for Mac OS X on Intel-based Macintosh computers

macosx.i386 for Mac OS X on PowerPC-based Macintosh computers

linux.x86 for the Linux computing platform

solaris2.sparc for Solaris on Sun Sparc computers

ibm for the IBM AIX computing platform

sgi for the SGI IRIX computing platform

To launch CHARICE, execute the shell script **<*path*>/charice** from a UNIX command line, and then click on the Virtual Machine splash window. Note that under Mac OS X, the X11 environment must be started prior to launching CHARICE.

Additional Notes

Regardless of the directory from which CHARICE is started, the default starting directory for file dialogs in CHARICE is always the directory in which **charice.sav** resides (unless changed in the CHARICE preferences). The “Start in” property of a shortcut or alias to CHARICE has no effect.

After your first use of CHARICE, a new file **charice_prefs.sav** will appear in the same directory as **charice.sav**. This file stores preference settings between uses. Default preference settings can be restored by deleting the file prior to starting CHARICE. If running directly from the CD-ROM, an error message will occur upon exiting CHARICE and preference settings will not be saved.

The following three subdirectories may also be copied from the CD-ROM.

1. **Documentation**: contains this report (**CHARICE_Manual.pdf**) as well as instructions for installing, using, and uninstalling the IDL Virtual Machine (**idlvm.pdf**).
2. **Examples**: contains all the files needed to run the example problems in Sections 5.1–5.4.
3. **EOS**: contains some useful EOS input files for various window and baseplate materials (see the file **README.txt** for details).

Please report any apparent bugs in CHARICE to the author by e-mail at **jpdavis@sandia.gov**.

Distribution

1 Dennis Hayes
P. O. Box 591
Tijeras, NM 87059

1 Jow-Lian Ding
Washington State University
School of Mech. and Materials Eng.
Pullman, WA 99164-2920

1 Lalit Chhabildas
Air Force Research Laboratory /MNMW
101 West Eglin Blvd, Suite 135
Eglin Air Force Base, FL 32542

3 Washington State University
Institute for Shock Physics
P. O. Box 642814
Pullman, WA 99164-2814
Attn: Y. M. Gupta
T. Jaglinksi
J. M. Winey

9 Los Alamos National Laboratory
P. O. Box 1663
Los Alamos, NM 87545
Attn: W. V. Anderson
F. J. Cherne
R. L. Gustavsen
R. S. Hixson
D. E. Hooks
B. J. Jensen
P. A. Rigg
S. Sheffield
D. G. Tasker

9 Lawrence Livermore National Laboratory
7000 East Ave.
Livermore, CA 94550
Attn: M. Bastea
G. W. Collins
J. H. Eggert
N. C. Holmes
J. O. Kane
J. H. Nguyen
D. A. Orlikowski
D. B. Reisman
R. F. Smith
K. S. Vandersall

1 Stephen Rothman
AWE, Aldermaston
Reading RG7 4PR
UNITED KINGDOM

1 Pierre-Louis Heréil
Délégation Générale pour l'Armement
Centre d'Etudes de Gramat
46500 Gramat
FRANCE

1 Christophe Voltz
Commissariat à l'Energie Atomique
Centre de Valduc
21120 Is sur Tille
FRANCE

Sandia Internal

1 MS-0836 M. R. Baer, 1500

1 MS-1106 T. Ao, 1646

1 MS-1168 M. D. Furnish, 1647
1 MS-1168 C. A. Hall, 1646

1 MS-1181 C. S. Alexander, 1647
1 MS-1181 J. R. Asay, 1646
6 MS-1181 J.-P. Davis, 1646
1 MS-1181 D. H. Dolan, 1646
1 MS-1181 M. D. Knudson, 1646
1 MS-1181 T. A. Mehlhorn, 1640
1 MS-1181 W. D. Reinhart, 1647
1 MS-1181 T. J. Vogler, 1647
1 MS-1181 J. L. Wise, 1646

2 MS-9018 Central Technical Files, 8944
2 MS-0899 Technical Library, 9536
1 MS-0161 Legal Intellectual Prop., 11500